June 2021
Volume 3
Issue 1

MERSIN PHOTOGRAMMETRY JOURNAL

The MERSİN PHOTOGRAMMETRY JOURNAL (MEPHOJ)

THE MERSİN PHOTOGRAMMETRY JOURNAL (MEPHOJ) publishes original and innovative contributions in photogrammetric applications ranging from the integration of instruments, methodologies, and technologies and their respective uses in the environmental sciences, engineering, and other natural sciences. Mersin Photogrammerty Journal is a branch of science that widely applied in many scientific disciplines. MEPHOJ aims to cover the entirety of Photogrammetry and Photogrammetric aplications about Geosciences, including their application domains. MEPHOJ strives to encourage scientists to publish experimental, theoretical, and computational results as detailed as possible so that results can be easily reproduced.

MEPHOJ is a double peer-reviewed (blind) OPEN ACCESS JOURNAL that publishes professional level research articles and subject reviews exclusively in English. It allows authors to submit articles online and track his or her progress via its web interface. All manuscripts will undergo a refereeing process; acceptance for publication is based on at least two positive reviews. The journal publishes research and review papers, professional communication, and technical notes. MEPHOJ does not charge for any article submissions or for processing.

CORRESPONDENCE ADDRESS
Journal Contact: myakar@mersin.edu.tr

CONTENTS

Volume 3 - Issue 1

RESEARCH ARTICLES

Mersin Photogrammetry Journal

https://dergipark.org.tr/en/pub/mephoj

e-ISSN 2687-654X

A combined use of image and range-based data acquisition for the three-dimensional information mapping archaeological heritage

Tuğba Sarıcaoğlu[*1], **Nezihat Köşklük Kaya** [2]

[1]*Dokuz Eylül University, The Graduate School of Natural and Applied Sciences, Department of Architecture, Izmir, Turkey*
[2]*Dokuz Eylül University, Faculty of Architecture, Architecture, Izmir, Turkey*

Keywords
Archaeological Heritage
Photogrammetry
Cloud-to-Cloud Distance
Orthophoto
Information Mapping

ABSTRACT

Acquisition of accurate archaeological heritage data is fundamental for the prospective steps of architectural conservation process. As of today, digital data capturing technologies such as image-based and range-based systems are rapidly becoming prevalent and generating digital surface representations of the object(s) in the form of three-dimensional point clouds. Point clouds assist heritage experts to carry out heritage analysis in digital forms, in particular to conduct condition assessment based on orthophotos of archaeological assets. In this paper, we introduce an integrated strategy by using Terrestrial Laser Scanning (TLS) and photogrammetry for the scope of obtaining orthophotos as basis for analyzing geometric, texture and color information of archaeological remains. Such a combination allows overcoming insufficiencies especially in terms of color due to the high natural light exposure. To remedy such visual obstacles, this paper demonstrates results to generate maximum visual data coverage of an archaeological heritage asset for the conservation process.

1. INTRODUCTION

Archaeological heritage fosters heterogeneous data types and information (Cipriani & Fantini, 2017). The scale of these data differentiates from microbiologic formation on a stone element to remains of an ancient mega structure. The surveying of these data to a maximum level plays a significant role for the sustainability of heritage information, hence the conservation process.

Immersive data acquisition technologies such as Terrestrial Laser Scanning (TLS) and photogrammetry provides accurate three-dimensional (3D) visualizations of the heritage assets` *as-is* state. Guidelines and strategies from suggestive studies have shown benefits of implementing TLS and photogrammetry in terms of high accuracy in the 3D recording of the archaeological heritage (English Heritage, 2011; Historic England, 2017). Surveying outputs, like point clouds and orthophotos, are essential to convert heritage data in architecturally elaborated datasets. With the help of these visual outputs, acquired data and information mapping about the asset could directly be represented and identified for heritage analysis (Chiabrando, Sammartano, & Spanò, 2016; Letellier, 2007). These visualizations could be presented either as 2D drawings and 3D models, and provide a basis for information mapping purposefully carried out (Santana-Quintero & Addison, 2007).

Heritage analysis illustrates, the material aspects, physical condition assessment of the remains and historical background of the assets` lifecycle (Arnold & Geser, 2008). The information assessment regarding building materials such as material types, decay patterns, deteriorations and failures is not only encouraged, but also strongly recommended for supporting the conservation process (ICOMOS, 1964, 1990, 1999). Digitally generated outputs have strong affordances as such actions. For instance, orthophoto based analysis of material types and deterioration patterns is a well-established approach in terms of conservation process (Cheng & Han, 2016; Chiabrando, Lo Turco, & Rinaudo, 2017; Dionísio, Martinho, Grangeia, & Almeida, 2013; Dore et al., 2015; Stanga et al., 2017). Orthophotos are particularly helpful for information mapping as the required surface, such as

* **Corresponding Author**

* tugbasaricaogluts@gmail.com) ORCID ID 0000 – 0001 – 7350 – 7142
(nezihat.koskluk@deu.edu.tr) ORCID ID 0000 – 0002 – 2124 – 3314

Cite this article

Sarıcaoglu T & Kaya N K (2021). A combined use of image and range-based data acquisition for the three-dimensional information mapping archaeological heritage. Mersin Photogrammetry Journal, 3(1), 01-09

Research Article / DOI: 10.53093/mephoj.891082

Received: 03/04/2021; Accepted: 29/05/2021

color and shape, data could be mirrored digitally. Such orthophotos should accommodate high-resolution properties and accurate colors to assess the visual aspects and support heritage analysis. To achieve that, data acquisition techniques and selection of surveying method play a critical role, defining the qualities of the surveyed data such as point clouds.

3D data capturing technologies provides accurate and precise dimensional digital visualizations of the heritage asset, with that acquisition methods heritage analysis is quite achievable. Yet, depending on the physical conditions sometimes this data could not be as salvageable in terms of analytic studies.

Furthermore, it is quite common to face data loss due to natural light exposure during TLS, which in turn creates a monochromic dataset, point cloud and orthophotos. Such a result is not viable when it comes to the 1:1 scale requirement when conducting archaeological heritage analysis.

This paper addresses maximizing the visual qualities of the orthophotos and illustrates the orthophoto rendering process and 3D model and proposes a strategy to combine TLS and photogrammetry to support heritage analysis, and in turn benefit conservation process. We focus on archaeological remains, in particular, work on the *Heroon* remains located at the *Erythrae* archaeological site, on the west coast of the Karaburun peninsula in Izmir, Turkey.

2. LITERATURE REVIEW

Digital data acquisition methods have been used in the field for over twenty years and are well recognized for surveying archaeological heritage subjects (Del Pozo et al., 2020; Fiorillo, Jiménez Fernández-Palacios, Remondino, & Barba, 2015; Şasi & Yakar, 2018, Yakar et al., 2010). These digital data acquisition techniques allow gathering 3D geometric point clouds, which are basically surface visualization of the object formed by 3D points with color data.

TLS method is among the most widely used technique for the reality-based documentation (Holden, Silcock, Arrowsmith, & Al Hassani, 2015), geometric and 3D textured visualizations purposes in the field (Fiorillo et al., 2015). Visualization of material deformation, structural monitoring and digital management are extended forms of TLS utilization for archaological heritage (Del Pozo et al., 2016; Fregonese et al., 2013).

Photogrammetric data acquisiton is widely acknowledged as an efficient documentation methods in the field, as well (Yilmaz, Yakar, Gulec, & Dulgerler, 2007). Moreover, photogrammetry has extensive usage from virtual reconstruction, material analysis, and to a small object modelling in the archaeological heritage (Pierdicca, Frontoni, Malinverni, Colosi, & Orazi, 2016; Porter, Roussel, & Soressi, 2019; Trizio, Savini, Giannangeli, Boccabella, & Petrucci, 2019).

These methods have advantages, but they are not free from limitations. Surveying archaeological heritage asset with TLS stands out as time consuming as well as costly since it requires tedious on-field setup, device maintenance, and highly priced equipment (Zeybek & Kaya, 2020). On the other hand, photogrammetric surveying is considered as cost-effective, accurate and easily accessible (Georgopoulos & Ioannidis, 2004; Zeybek, Şanlıoğlu, & karauğuz, 2013).

Nevertheless, only a few studies extend these innovative applications to professionally applicable use complementary to conservation process. For instance, Corso, Roca, & Buill (2017) suggests a methodology to illustrate material loss on a 13th century Cathedral using TLS point cloud and generated orthophotos. Another research shows weathering on a 12th century church facade, from orthophotos rendered by TLS point cloud which are supported with radiographical sensory device (Del Pozo et al., 2016). Gaiani and others (2017) propose a methodology to automatically provide color equalization of an 16th century heritage building by photogrammetry. In that research, authors use color checkers and have more realistic chromatic representation of the building's façade surface with corrected texture map. Even though, Gaiani et al. (2017) achieves a color fidelity, the results are limited to 3D facade visualizations.

Although, these studies successfully represent geometric accuracy and façade pathologies by using point clouds, texture maps and orthophotos, cannot fully foster a semantic 3D dimensionality in the scale of archaeological heritage, especially in the archaeological remains which are Greek or older. In such cases, there is a lack of dominant verticality (such as facades), and the research methods offered for successful condition assessment of building facades for architectural conservation, fail to respond the needs of efficiently documenting archaeological remains elaborately for analysis.

3. METHOD

In this paper, we offer 3D textured visualizations as surface modellings and methodology benchmarking by the integrated use of TLS and photogrammetry to provide effective and accurate visual outputs for heritage analysis. We focus on the combination of two surveying methods potential for heritage analysis, particularly for archaeological heritage dating before the *Common Era*. Our research differs from the previous research on two counts: 3D data acquisition and developing semantic surface image renderings. We chose TLS as for the primary surveying but resulting data was not salvageable enough for an archaeological heritage asset. That prompted us to re-surveying, we implemented ground-based photogrammetry to compensate the gap in the data. In addition to surveying decision, we rendered ample amounts of orthophotos as parallel to every surface both horizontally and vertically to have information mappings on the assets` modelled survey, not to have textured 3D representation of the survey data. More importantly, our case, dating back to 4th century BC, requires a different approach of representation due to its historical and physical characteristics of *in-situ* remains. Besides, calling the case *Heroon*, we think a Greek temple like building, which is architecturally distinctive with respect to its scale, construction system and material aspects.

Architecturally, this kind of typology requires a close look at the element scale in the conservation process. For example, Heroon had walls, but *in-situ* remains should be evaluated stone by stone. As a result of these particularities, the surveyed data management is dissimilar to the studies mentioned in Section 2.

4. *IN-SITU* REMAINS OF THE *HEROON*

The *Heroon* remain is situated at the northern part of the archaeological site of *Erythrae* (Figure 1, Figure 2)). The remains occupy a rectangular area of 10 by 18 meters at sides.

A scripted graph, points the main construction dates to 4th BC (Engelmann & Merkelbach, 1972). The meaning of the *Heroon* originates from the word 'heroin', and signifies sacred places in the forms of temple-like tombs of important people of the time (Andronikos, 1980). Nevertheless, there is no further information regarding its historical background. In fact, the scarcity of the information is not limited to that, there is also no architectural documentation of the remains since its discovery in 1965.

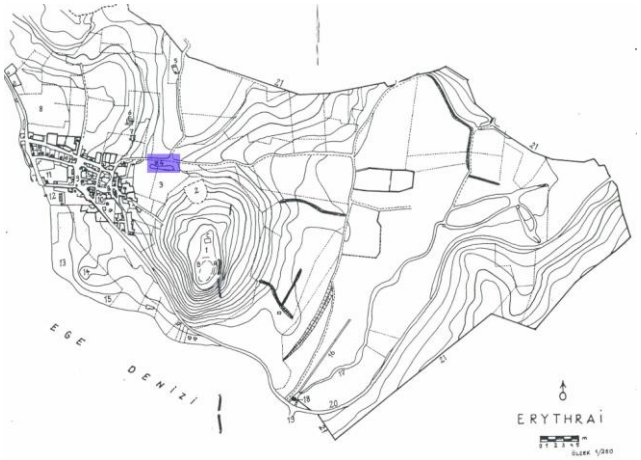

Figure 1. Location of the Heroon in Erythrae, based on the map by Akurgal (1979)

Figure 2. A drone image of the Heroon from above in 2019 (taken by the excavation team)

5. SURVEYING CAMPAIGN – KEY ASPECTS

In this paper, we focus on the data acquisition, from raw data like geometric values (i.e., height and depth) to metadata such as point cloud and orthophotos, of the in-situ remains. We carried out data acquisition at the location in two campaigns first by TLS in August 2019, and second by photogrammetry in November 2019. Our paper does not extend to any coupling with an excavation campaign since the remains are on private property.

We planned the survey for the requirement of 1:1 drawing scale. We used *TLS FARO Focus S 350* for TLS which provides under 2mm measurement accuracy (URL-1). Additionally, for the second surveying, we worked with ground-based photogrammetry (with *Canon EOS 200D*) method to benefit from 4-10 mm at 100m geometric accuracy that it could afford (Vanneschi, Eyre, M., & Coggan, 2017). The workflow of this approach is as follows; I) data acquisition, ii) point cloud generation, iii) point cloud alignment, iv) orthophoto rendering and v) model concept.

5.1. Data Acquisition

5.1.1. Terrestrial Laser Scanning

We scanned the *Heroon* by renting *Faro Focus S350* terrestrial laser scanner in August 2019. Scanning took place with 24 colored scan positions (Figure 3). Target spheres and target papers was placed in the scanned area for registration purposes. Each scan lasted between 8 to 9 minutes and resolution parameters set to ½ (high) (Table 1).

Table 1. TLS Parameters

Faro Focus S 350	
Resolution	1/2 (High)
Quality	2x
Scan Time	8-9 mins
Angular Area (Vertical)	90^0 to -60^0
Angular Area (Horizontal)	0^0 to 360^0
Target Type	Sphere and Paper
Coordinate System	Local (GPS)

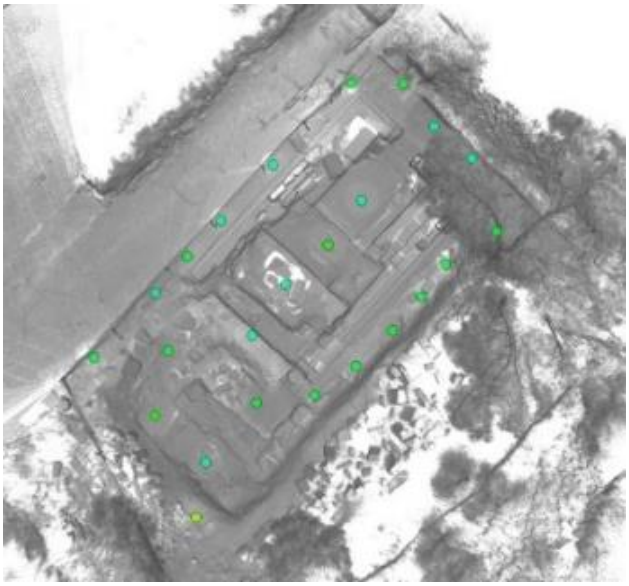

Figure 3. The scan positions (green dots), and gray scaled point cloud of the Heroon remains.

After that, we imported the raw scans through the scanner`s processing software, *Scene*, and processed and performed registration. Following scan registration, point cloud data rendered reaching 680 million points. Although, surface geometry generated to test the point cloud was favorably accurate and factual, the point

cloud itself was not be sufficiently colored due to the high intensity of the natural light exposure during the scanning process. That showed insufficient results in testing as almost monochromic orthophotos, which creates an obstacle for the next steps of the research. To mitigate the data gap, we revisited and performed with photogrammetry in November 2019.

5.1.2. Ground-based Photogrammetry

For the ground-based photogrammetry, we used Canon EOS 200D DSLR camera with 35mm fixed lens (Table 2). We gathered 2709 photographs in JPG format, of each overlapping at least two-third of the previous one for the maximum convenience of the photogrammetric survey as well as the *Agisoft Metashape Professional* (Version 1.5.2) photogrammetry software (Agapiou & Georgopoulos, 2006). *Agisoft Metashape* allows automatic generation of a sparse cloud based on the structure from the motion (SfM) algorithm (URL-3).

The white balance of the images has been decided in accordance with the built-in auto ambient priority of the camera considering the climatic condition of the site which was dry and unpolluted in consequence of previous rainfalls.

Table 2. Canon EOS 200D Specifications (URL-2)

EOS 200D 24.2MP DSLR Camera	
Effective Pixels	24.2 P
Sensor Type	CMOS
Sensor Size	22.3 x 14.9mm
Focal Length	f/2.8
ISO Rating	ISO 100 - 25600
Image Processor	DIGIC 7

Following the fieldwork, we imported raw images into the *Agisoft Metashape* photogrammetry software for the alignment. We aligned photos in one chunk, also rendered sparse point cloud with medium accuracy setting selected (Figure 4). This process took 14 hours with 16 GB RAM configurated computer. At the time of photogrammetric data capturing, we could not measure control points with a total station since the equipment was not available. Instead, we re-used the coordinates of 11 targets from TLS scans by importing them before the dense cloud calculation. Next, with medium accuracy and aggressive filtering mode, we built dense point cloud (almost 78 million points) in a process taking 24 hours. In addition, we cleaned and decluttered off the noise to generate the final point cloud of the *Heroon* remains.

5.2. Point Cloud Alignment

We could achieve accurate scale and dimension thus the real orientation of the surveyed object by implementing control points. Some studies suggest using a geodetic device to record geoinformation of the control points and in the photogrammetry process in order to scale and orient the point cloud (Yakar & Yılmaz, 2008; Yıldız et al., 2011). However, in this research, due to the equipment limitations, we realized georeferencing manually. In order to achieve maximum level of accuracy, we used the data from TLS point cloud as a base by first exporting 11 distinct points in the TLS point cloud, and then converting them into .csv format. Subsequently, we imported the same control points into *Agisoft Metashape* over the course of dense cloud building phase (Figure 5, Figure 6) and used them as 'markers' in *Agisoft Metashape* before dense cloud rendered. That procedure provided setting of the photogrammetric point cloud georeferencing based on the in-house TLS point cloud; therefore, alignment is concluded (Figure 7).

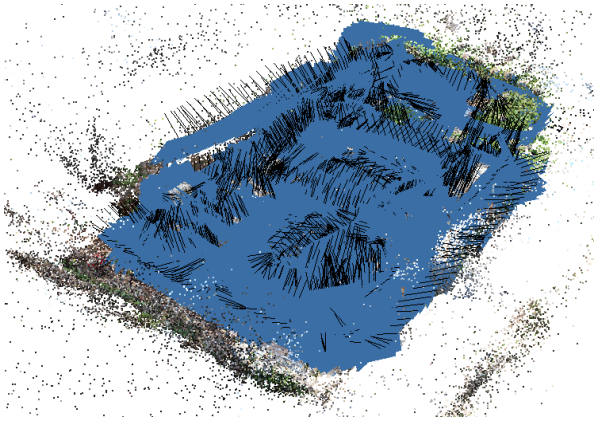

Figure 4. Photogrammetric survey workflow; a) Camera positions, and b) sparse point cloud

Control point implementation helped georeferencing the point cloud. Yet, we calculated cloud-to-cloud distance to check on this alignment for the data accuracy. We used *CloudCompare* (Version 2.11.3) to perform *cloud-to-cloud* distance calculation in accordance with the set workflow (URL-5). We converted both TLS and photogrammetric point cloud into. E57 file format as it fosters both RGB and three-dimensional location data.

Imported point clouds subjected to cloud-to-cloud distance tool (URL-5). This tool calculates two or more clouds according to the user-based area of interest from the point cloud data. First, base point cloud decided, in this case TLS point cloud. Octree level, built-in subdivision parameter of the point cloud, is set to be auto. Following, cloud-to-cloud distance tool activated and performed (Figure 8).

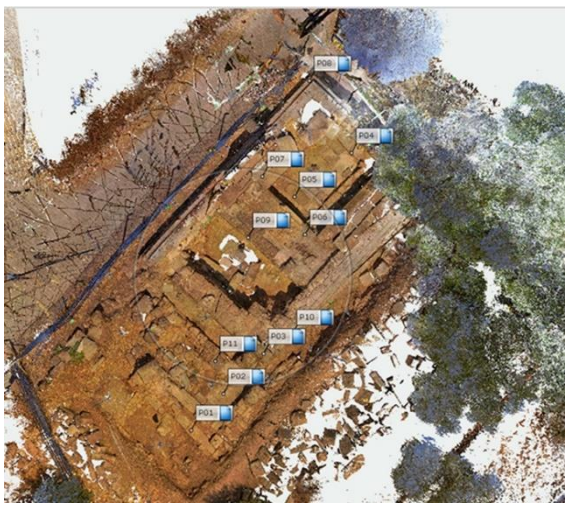

Figure 5. Alignment workflow of the point clouds; data from TLS.

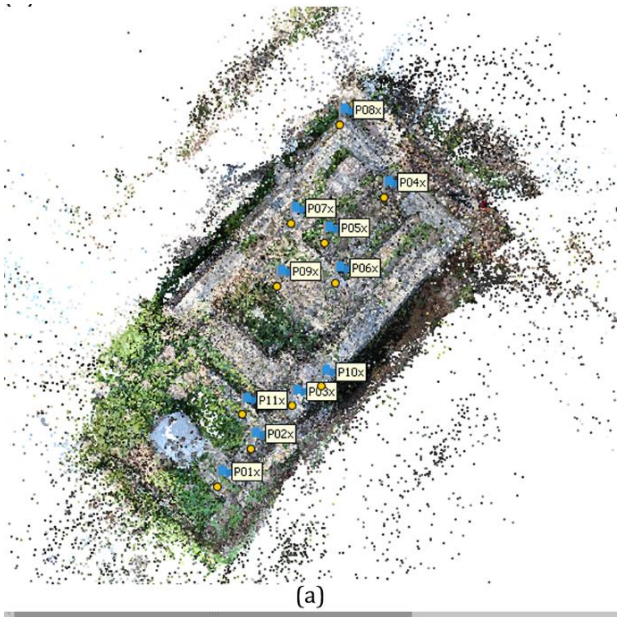

Markers	X (m)	Y (m)	Z (m)	Accuracy (m)	Error (m)	Projections	Error (pix)
P01x	16.772970	28.029010	440.661430	0.005000	0.053869	10	0.318
P02x	30.324180	43.458310	439.713440	0.005000	0.043362	16	0.256
P03x	46.991510	60.623030	448.030320	0.005000	0.020725	19	0.718
P04x	84.156400	145.142730	437.517280	0.005000	0.030165	35	0.901
P05x	60.140450	126.657340	436.014560	0.005000	0.035965	15	0.641
P06x	64.543310	110.425040	442.590980	0.005000	0.052833	5	0.650
P07x	46.620030	134.594570	447.987060	0.005000	0.039142	10	0.887
P08x	66.067060	174.605430	446.128080	0.005000	0.049923	11	0.251
P09x	40.689130	109.270050	442.829130	0.005000	0.066763	4	0.282
P10x	58.871630	68.642900	445.590130	0.005000	0.023498	34	0.225
P11x	26.974190	57.337360	440.616610	0.005000	0.033754	13	0.385
Total Error							
Control points					0.043043		0.596

(b)

Figure 6. Alignment workflow of the point clouds; a) imported .csv into Agisoft Metashape, b) x, y, z values of the implemented control points.

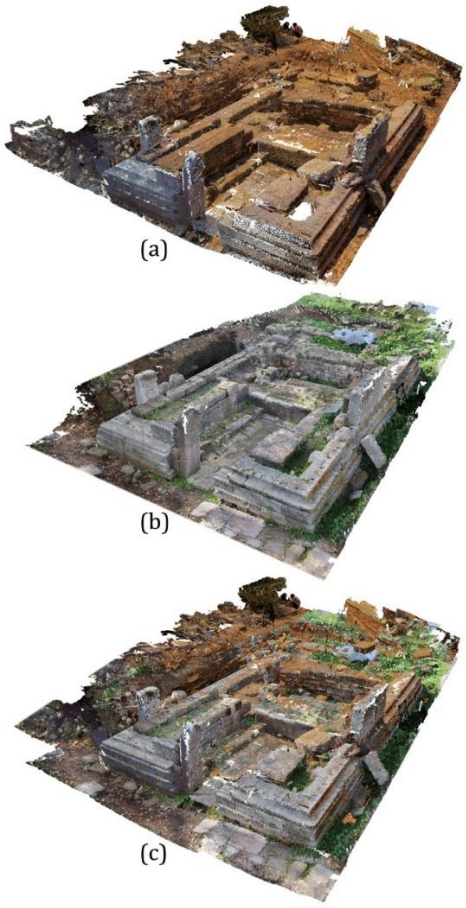

Figure 7. Generated and aligned point clouds, (a) TLS, (b)Photogrammetry, (c) TLS& Photogrammetry.

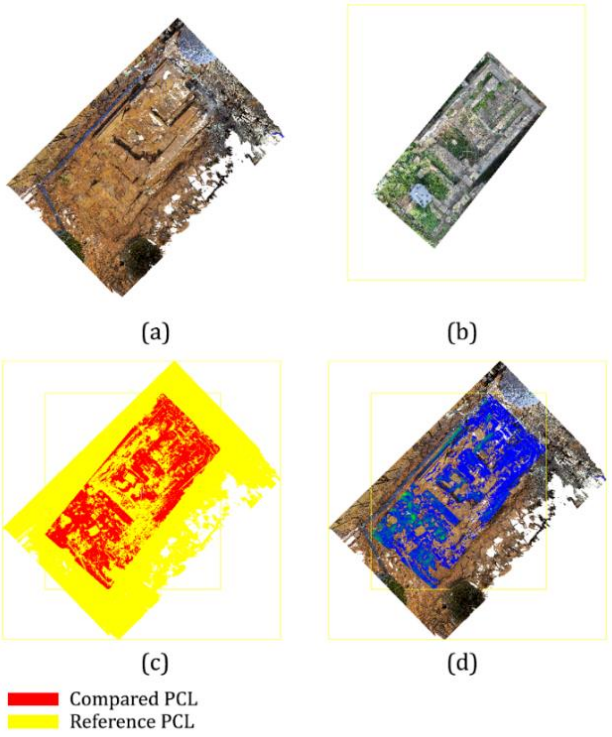

Figure 8. Cloud-to-cloud distance computing process, (a) TLS point cloud, (b) photogrammetry point cloud, (c) comparison decisions, (d) TLS and photogrammetry point cloud overlap.

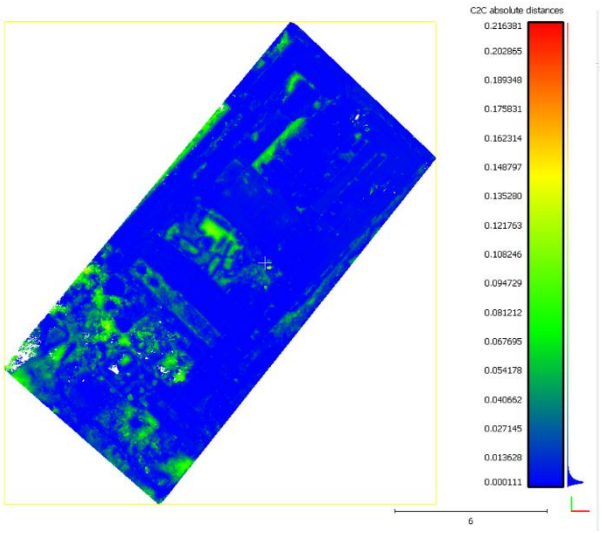

Figure 9. Computed result with scalar field`s color scale, meters.

According to the final calculation graphic, blue represents maximum overlapping points and red *vice versa*, green, areas are the vegetation due to rainfall on the in-situ remains (Figure 9). The maximum distance (non-visible red areas on green vegetation) is under 22 cm, minimum distance is under 1mm.

5.2.1. Orthophoto Rendering

Following the georeferencing of point clouds, their alignment and calculation, we decided resulting photogrammetric point cloud is comprehensive enough to render orthophotos of the remains.

We used *PointCab* (Version 3.9), point cloud processing software, to generate the orthophotos. TLS point cloud and photogrammetric point cloud processed

in the *PointCab* separately. Since the purpose of the photogrammetric survey was to compensate the TLS`s data gap, we set orthophoto rendering parameters constant for both operations (TLS and photogrammetry).

PointCab renders orthophotos with axis-based projection settings. User could decide position of the axis and then sets the parameters as required. The *Heroon*`s building line is $47^0$ to $43^0$ according to the TLS survey. As a result of that, we set the axis` angles as -133^0, -43^0, 137^0, and 47^0, for the orthophoto operations to create parallelly projected rectified images (Figure 10-11-12).

To create mutually complementary orthophotos, we set the same parameters for each of the section and layout axis. Position of the axis of the section and layout is critically vital to create constant point projections; therefore, we first decided on TLS then carried the same x, y, z, angle, and orientation data on photogrammetric point cloud. Furthermore, we set the image resolution to 2mm, zero reflectivity and 100% color for processing each orthophoto. Also, for the CAD parameters, we decided on white background, PNG format, metric unit system and 3D projection. All in all, we generated more than 400 orthophotos between the separately obtained point clouds. In this way, formed orthophotos became compliable and interchangeable, which is critical to remedy data loss from the original TLS survey.

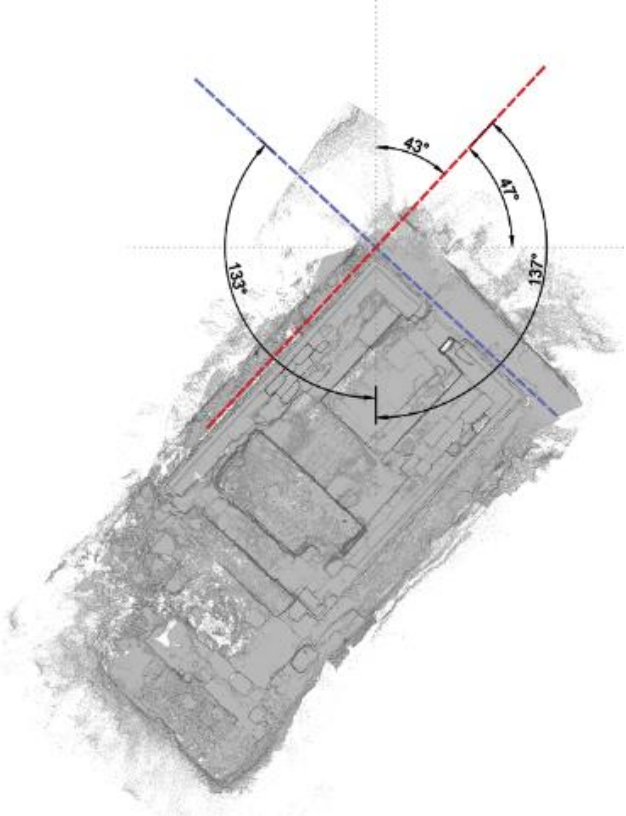

Figure 10. Projection angle for orthophoto rendering process, on photogrammetric point cloud.

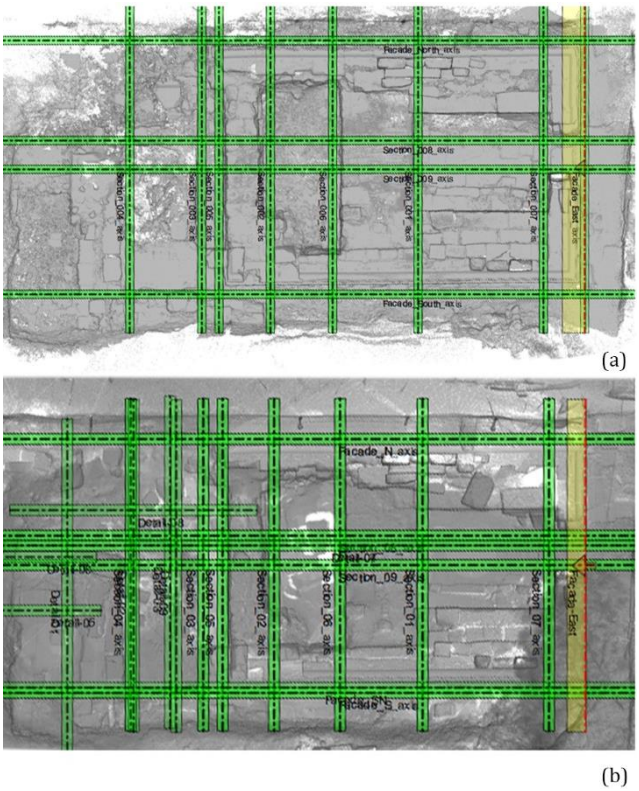

Figure 11. Orthophoto rendering process (47^0 flipped for visual purposes), section axis are green lines, (a) photogrammetry point cloud, (b) TLS point cloud.

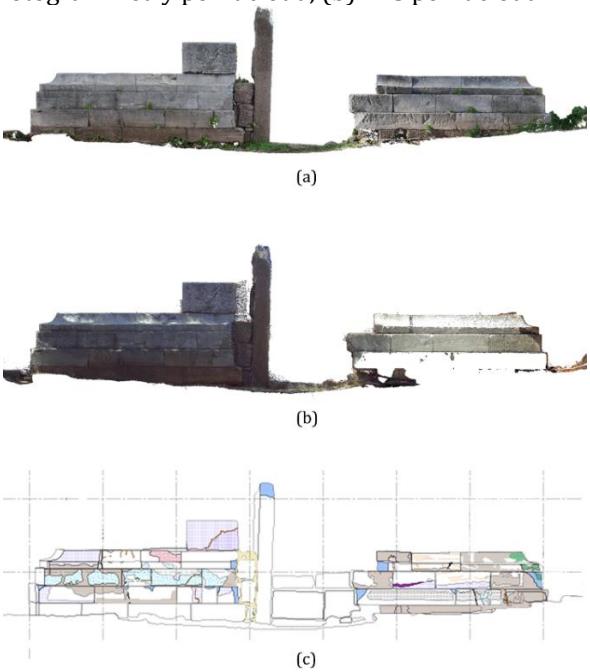

Figure 12. East elevation orthophotos of the in-situ remains, generated from (a) photogrammetry and (b) TLS, and (c) information mapping of material deteriorations.

6. RESULTS

Surveying an existing geometry is easily practicable with the implementation of digital data capturing procedures. Eminently, both image-based and range-based methods have been implemented on the same object in this research. That resulted in two different datasets which are aligned and scaled and prepared to be utilized for the next steps in the holistic conservation

process (Table 3). Most importantly, we managed to cover the data gap such as in the color or texture from the first survey, TLS, with implementing second one, photogrammetry.

Table 3. Data Acquisition Processing

Methods	TLS	Photogrammetry
Area (WxLxD)m	33x23x5	9.7x19.3x2.7
Data acquisition time	24 hrs.	40hrs.
Acquisition Locations	24 Scans	2709 Images
Resulted Datasets	PCL(680mm)	PCL(72mm)
White Balance	Not Appl.	AAP*

*Auto Ambient Priority

Terrestrial laser scanning covered larger environmental data. Also, the scanned surface representation was quite dense. However, due to natural light exposure, some shading and monochromic color recording has occurred. TLS being a rapid and robust surveying method provided the field work to finish less than 8 hours. Yet, also resulted with ample of redundant data recording such as tree leaves and even flying birds. Thus, the data had too much noise and we had to devote an extensive time in data cleaning while registering the scans. Although, we tried to implement auto white balance to the scans, in *Scene*, that was not impeccable to continue due to shadings became more obvious in the scans and created data liability. It is also worth mentioning that rapid scanning cost partially data loss of the Heroon remains, too.

The photogrammetric survey was particularly effective for graphically strong orthophoto generation. However due to not having access to a geodesic device, point cloud generation took time in terms of georeferencing. In this paper, we particularly tried to solve this issue manually yet meaningfully. To do so, we specified control points from registered TLS point cloud and converted and imported them into Agisoft Metashape during photogrammetric point cloud generation. That immensely help to reduce scale and positional errors for photogrammetric survey. In addition to manual control point implementation, we performed cloud-to-cloud distance with CloudCompare, which proved the validity of the aligned photogrammetric point cloud (Figure 13).

Orthophoto generation of the *Heroon* ensured extensive metadata for the conservation process, analysis, of the heritage asset. Aligned point clouds with relevant accurate orthophotos played a significant role for information mapping of the remains` material and condition assessment.

7. CONCLUSIONS

In this paper, we illustrated three-dimensional data acquisition methods for an archaeological heritage. Particularly, we attempted to combine the TLS and photogrammetric data acquisition, offering an alignment in the workflows to reach accurate and reliable 3D representation of heritage and accurate representation in orthophotos. Information mapping of the Heroon remains, material culture and condition, is digitally visualized by point clouds, and off rendered orthophotos.

Our technique shows a clear advantage over terrestrial laser scanning in terms of texture detail of the orthophoto dataset. The evidence from this study suggests, even after geometrically accurate but off textured survey data acquisition, image-based cost-effective surveying could remedy this issue. We have managed to do information mapping and 3D modelling of the Heroon holistically with highly detailed and precise survey datasets.

It is crucial to note the data acquisition actions, as well as the methods, could be distinctive depending on the specifications of the heritage itself and the opportunities to research on, but in the end, the generation of accurate heritage data to use as a basis for conservation actions remain fundamental.

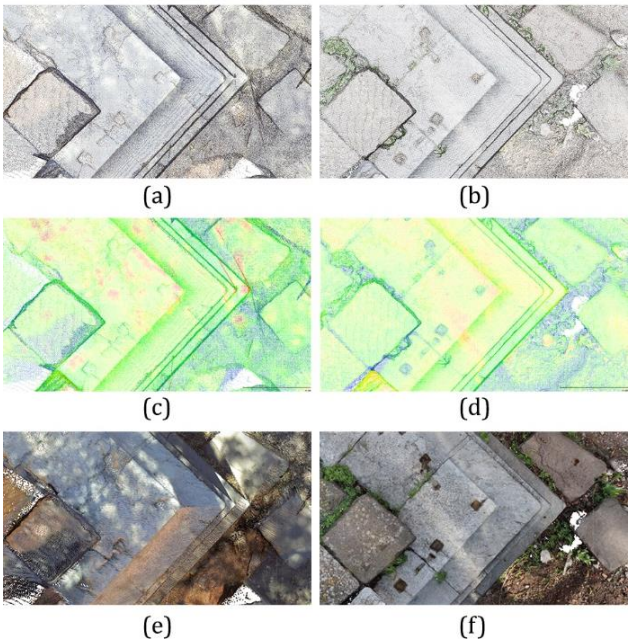

Figure 13. Core data of rendered orthophotos (a) TLS point cloud, (b) photogrammetric point cloud, (c) TLS scalar field, RGB, (d) Photogrammetry scalar field, RGB, (e)TLS orthophoto, (f) photogrammetric orthophoto.

ACKNOWLEDGEMENT

This study is a part of an ongoing dissertation investigating archaeological heritage building information modelling (HBIM) as holistic data-driven conservation process methodology. The authors would like to express their thanks to Dr. Ayşe Gül Orbay for enabling the site survey, and Dr. Öncü Başoğlan Avşar and Dr. Ali Öz for the valuable discussions in the committee meetings.

Author contributions

Tuğba Sarıcaoğlu: Collected the data, Performed the analysis and synthesis, Wrote the paper, designed the methodology; **Nezihat Köşklük Kaya:** Supervised the progress, Contributed the data representation

Conflicts of interest:

The authors declare no conflicts of interest.

REFERENCES

Agapiou A & Georgopoulos P A (2006). Photogrammetric Potential of Digital Cameras in Handheld Gadgets for Digital Close Range Applications. *Heritage*, 1–6.

Akurgal E (1979). *Erythrai an Ancient Ionian City*. Izmir.

Andronikos M (1980). 'The Royal Tombs at Vergina' The Search for Alexander. *The Royal Graves at Vergina*, 26(5).

Arnold D & Geser G (2008). EPOCH Research Agenda for the Applications of ICT to Cultural Heritage. Full Report. *Epoch*, (May), 244. Retrieved from http://www.epoch-net.org/index.php?option=com_content&task=view&id=200&Itemid=306

Cheng G & Han J (2016). A Survey on Object Detection in Optical Remote Sensing Images. *ISPRS Journal of Photogrammetry and Remote Sensing*, 117, 11–28. Retrieved from https://doi.org/10.1016/j.isprsjprs.2016.03.014

Chiabrando F, Lo Turco M & Rinaudo F (2017). Modeling the Decay in an HBIM Starting from 3D Point Clouds. A Followed Approach for Cultural Heritage Knowledge. In *International Archives of the Photogrammetry, Remote Sensing and Spatial Information Sciences - ISPRS Archives* (Vol. 42). Retrieved from https://doi.org/10.5194/isprs-archives-XLII-2-W5-605-2017

Chiabrando F, Sammartano G & Spanò A (2016). Historical Buildings Models and Their Handling via 3D Survey: From Points Clouds to User-oriented HBIM. In *International Archives of the Photogrammetry, Remote Sensing and Spatial Information Sciences - ISPRS Archives* (Vol. 41). Retrieved from https://doi.org/10.5194/isprsarchives-XLI-B5-633-2016

Cipriani L & Fantini F (2017). Digitalization Culture vs Archaeological Visualization: Integration of Pipelines and Open issues. *International Archives of the Photogrammetry, Remote Sensing and Spatial Information Sciences - ISPRS Archives*, 42(2W3), 195–202. Retrieved from https://doi.org/10.5194/isprs-archives-XLII-2-W3-195-2017

Corso J, Roca J & Buill F (2017). Geometric Analysis on Stone Façades with Terrestrial Laser Scanner Technology. *Geosciences (Switzerland)*, 7(4), 1–12. Retrieved from https://doi.org/10.3390/geosciences7040103

Del Pozo S, Herrero-Pascual J, Felipe-García B, Hernández-López D, Rodríguez-Gonzálvez P & González-Aguilera D (2016). Multispectral Radiometric Analysis of Façades to Detect Pathologies From Active and Passive Remote Sensing. *Remote Sensing*, 8(1). Retrieved from https://doi.org/10.3390/rs8010080

Del Pozo S, Rodríguez-Gonzálvez P, Hernández-López D, Onrubia-Pintado J, Guerrero-Sevilla D & González-Aguilera D (2020). Novel Pole Photogrammetric System for Low-cost Documentation of Archaeological Sites: The Case Study of 'Cueva Pintada'. *Remote Sensing*, 12(16). Retrieved from https://doi.org/10.3390/RS12162644

Dionísio A, Martinho E, Grangeia C & Almeida F (2013). Examples of the use of non-invasive techniques for the evaluation of stone decay in Portugal. *Key Engineering Materials*, 548(May), 239–246. Retrieved from https://doi.org/10.4028/www.scientific.net/KEM.548.239

Dore C, Murphy M, McCarthy S, Brechin F, Casidy C & Dirix E (2015). Structural Simulations and Conservation Analysis-Historic Building Information Model (HBIM). In *International Archives of the Photogrammetry, Remote Sensing and Spatial Information Sciences - ISPRS Archives* (Vol. 40). Retrieved from https://doi.org/10.5194/isprsarchives-XL-5-W4-351-2015

Engelmann H & Merkelbach R (1972). *Die Inschhriften von Erythrai und Klazomenai*. Bonn: R.Habelt.

English Heritage. (2011). 3D Laser Scanning for Heritage, 1–41.

Fiorillo F, Jiménez Fernández-Palacios B, Remondino F, & Barba S (2015). 3D Surveying and modelling of the Archaeological Area of Paestum, Italy. *Virtual Archaeology Review*, 4(8), 55. Retrieved from https://doi.org/10.4995/var.2013.4306

Fregonese L, Barbieri G, Biolzi L, Bocciarelli M, Frigeri A, & Taffurelli L (2013). Surveying and Monitoring for Vulnerability Assessment of an Ancient Building. *Sensors (Basel, Switzerland)*, 13(8), 9747–9773. Retrieved from https://doi.org/10.3390/s130809747

Gaiani M, Apollonio F I, Ballabeni A & Remondino F (2017). Securing Color Fidelity in 3D Architectural Heritage Scenarios. *Sensors*, 17(11). Retrieved from https://doi.org/10.3390/s17112437

Georgopoulos A & Ioannidis C (2004). Photogrammetric and Surveying Methods for The Geometric Recording of Archaeological Monuments. *FIG Working Week*, 22–27.

Historic England. (2017). Photogrammetric Applications for Cultural Heritage. *Guidance for Good Practice*, 1–124.

Holden L D, Silcock D M, Arrowsmith C A & Al Hassani M (2015). Laser Scanning for The Documentation and Management of Heritage Sites Within the Emirate of Fujairah, United Arab Emirates. *Arabian Archaeology and Epigraphy*, 26(1), 55–67. Retrieved from https://doi.org/10.1111/aae.12050

ICOMOS (1964). The Venice Charter 1964. *IInd International Congress of Architects and Technicians of Historic Monuments*, 1–4.

ICOMOS (1990). Arkeolojik Mirasın Korunması ve Yönetimi Tüzüğü. Lozan (Lausanne): ICOMOS. Retrieved from https://www.icomos.org/en/practical-information/179-articles-en-francais/ressources/charters-and-standards/160-charter-for-the-protection-and-management-of-the-archaeological-heritage

ICOMOS (1999). Principles for the Preservation of Historic Timber Structures (1999). *Icomos*, (October), 2–4.

Letellier R (2007). *Recording and Information Management for the Conservation of Heritage Places: Guiding Principles*. *Heritage* (Vol. Guiding pr).

Pierdicca R, Frontoni E, Malinverni E S, Colosi F & Orazi R (2016). Virtual Reconstruction of Archaeological Heritage Using A Combination of Photogrammetric Techniques: Huaca Arco Iris, Chan Chan, Peru. *Digital Applications in Archaeology and Cultural Heritage*, 3(3), 80–90. Retrieved from https://doi.org/10.1016/j.daach.2016.06.002

Porter S T, Roussel M & Soressi M (2019). A Comparison of Châtelperronian and Protoaurignacian Core Technology Using Data Derived from 3D Models. *Journal of Computer Applications in Archaeology*, 2(1), 41–55. Retrieved from https://doi.org/10.5334/jcaa.17

Sanlıoğlu İ, Zeybek M & Karauğuz G (2013). Photogrammetric survey and 3D modeling of Ivriz Rock relief in late hittite era. *Mediterranean Archaeology and Archaeometry*, 13, 147–157.

Santana-Quintero M & Addison A C (2007). Digital Tools for Heritage Information Management and Protection: The Need of Training. In *Proceedings of the 13th International Conference on Virtual Systems and Multimedia* (pp. 35–46). Berlin, Heidelberg: Springer-Verlag.

Şasi A & Yakar M (2018). Photogrammetric Modelling of Hasbey Dar'ülhuffaz (Masjıd) Using an Unmanned Aerial Vehicle. *International Journal of Engineering and Geosciences*, 3, 6–11. Retrieved from https://doi.org/10.26833/ijeg.328919

Stanga C, Spinelli C, Brumana R, Oreni D, Valente R & Banfi F (2017). A N-D Virtual Notebook about the Basilica of S. Ambrogio in Milan: Information Modeling for the Communication of Historical Phases Subtraction Process. *International Archives of the Photogrammetry, Remote Sensing and Spatial Information Sciences - ISPRS Archives*, 42(2W5), 653–660. Retrieved from https://doi.org/10.5194/isprs-archives-XLII-2-W5-653-2017

Trizio I, Savini F, Giannangeli A, Boccabella R & Petrucci G (2019). The Archaeological Analysis of Masonry for The Restoration Project In HBIM. *ISPRS - International Archives of the Photogrammetry, Remote Sensing and Spatial Information Sciences*, XLII-2/W9, 715–722. Retrieved from https://doi.org/10.5194/isprs-archives-XLII-2-W9-715-2019

Vanneschi C, Eyre M, Francioni M & Coggan J (2017). The Use of Remote Sensing Techniques for Monitoring and Characterization of Slope Instability. *Procedia Engineering*, 191, 150–157. Retrieved from https://doi.org/10.1016/j.proeng.2017.05.166

Yakar M & Yılmaz H M (2008). Kültürel Miraslardan Tarihi Horozluhan'ın Fotogrametrik Rölöve Çalışması Ve 3 Boyutlu Modellenmesi. *Selçuk Üniversitesi Mühendislik, Bilim Ve Teknoloji Dergisi*. SELÇUK ÜNİVERSİTESİ MÜHENDİSLİK FAKÜLTESİ DEKANKLIĞI SELÇUKLU KONYA: Konya Teknik University.

Yakar M, Yılmaz H M, Yıldız F, Zeybek M, Şentürk H & Çelik H (2010). Silifke-Mersin Bölgesinde Roma Dönemi Eserlerinin 3 Boyutlu Modelleme Çalışması ve Animasyonu. *Jeodezi ve Jeoinformasyon Dergisi*. TMMOB Harita ve Kadastro Mühendisleri Odası Sümer 1. sokak No:12/4 06440 Kızılay/Ankara: TMMOB Harita ve Kadastro Mühendisleri Odası.

Yılmaz H M, Yakar M, Güleç S A & Dulgerler O N (2007). Importance of digital close-range photogrammetry in documentation of cultural heritage. *Journal of Cultural Heritage*, 8(4), 428–433. Retrieved from https://doi.org/10.1016/j.culher.2007.07.004

Yıldız F, Yakar M, Zeybek M, Kocaman E, Pınar K, Telci A, Mutluoglu O & Yılmaz H M (2011). Dağpazari Kilisesi (Mut¬Mersin) Rölöve Örneği. In *TMMOB Harita ve Kadastro Mühendisleri Odası 13. Türkiye Harita Bilimsel ve Teknik Kurultayı*. Ankara: TMMOB.

Zeybek M & Kaya A (2020). Tarihi Yığma Kiliselerde Hasarların Fotogrametrik Ölçme Tekniğiyle İncelenmesi: Artvin Tbeti Kilisesi Örneği (Investigation of Damages in Historical Masonry Churches with Phtogrammetric Measurement Techniques: A Case Study of Artvin Tbeti Church). *Geomatik*, 5, 51–63. Retrieved from https://doi.org/10.29128/geomatik.568584

URL-1.https://www.laserscanning europe.com/en/news/faro-focus-s-150-s-350-what-improvements-over-the-predecessor-models-faro-focus-x-130-x-330

URL-2.https://gadgets.ndtv.com/canon-eos-200d-24-2mp-dslr-camera-11662

URL-3.https://guides.lib.unc.edu/metashape

URL-4.https://www.faro.com/en/Resource-Library/Case-Study/replace-your-total-station-with-a-3d-laser-scanner

URL-5. https://www.cloudcompare.org/doc/wiki/index.php?title=Cloud-to-Cloud_Distance

Mersin Photogrammetry Journal
https://dergipark.org.tr/en/pub/mephoj
e-ISSN 2687-654X

Digital documentation of ancient stone carving in Şuayip City

Halil İbrahim Şenol*[1], Nizar Polat [1], Yunus Kaya [1], Abdulkadir Memduhoğlu [1], Mustafa Ulukavak [1]

[1]*Harran University, Engineering Faculty, Department of Geomatic Engineering, Şanlıurfa, Turkey*

Keywords
SfM
Photogrammetry
Şuayip City
Archaeology

ABSTRACT

Şanlıurfa is an important archaeological and cultural region where people have left permanent artifacts dating back to 12 thousand years. For this reason, it is very important to record and document the artifacts in this region where cultural heritage is very intense. With the developing technology, it has become easier to document historical artifacts and to transfer them to future generations. In this direction, historical artifacts can be recorded easily and accurately with the photogrammetry technique, which is one of the important tools offered by developing technology. With this method, a detailed model of the historical artifact can be created and recorded in the digital environment. In this study, a point cloud and a 3D model of a carving stone, located in the region known as Şuayip City, located 80 km south of Şanlıurfa, was produced by photogrammetry, and the details of the carving stone were revealed. At the result of the study, the carving on the stone was revealed by using various filtering techniques.

1. INTRODUCTION

Cultural heritages unearthed in archaeological sites allow us to obtain information about past civilizations and to experience the spirituality of those times (Eskikurt, 2003; Yakar et al. 2015; Kaya et al., 2021). Also, it is an obligation to pass on the works of past civilizations to future generations. The efforts of human beings to leave a mark on the places they have lived since their existence make it possible for us to reach these artifacts after many years. Cultural heritage sites have great importance in terms of both cultural tourism and ongoing scientific studies in these areas. Cultural heritages can be examined under three headings as concrete, intangible and natural heritages (Ulvi et al., 2019a). Thanks to tangible cultural heritages such as painting, sculpture, buildings, clothing, and objects, it can be seen to what extent the daily lives and civilizations of the communities that lived in the past have progressed. While the materials from which the objects found in the archaeological areas are conveyed to us the conditions of that day, artistic structures such as painting, and sculpture are also a message from the past centuries to the present.

Historical artifacts are in danger of being damaged or destroyed over time due to natural or human factors (Cömert et al., 2012; Tercan, 2017). Documentation of cultural heritage has gained momentum in parallel with the development of technology. Documentation of cultural heritages allows both the object features to be examined in more detail and to be recorded and to take measures against disruptions such as accidents and natural disasters that may occur in the coming years. Many methods have been used to document small objects or large structures that can count as cultural heritage. However, when the studies in the literature are examined, it is seen that taking pictures is easier than other methods (Yakar et al. 2016; Ulvi et al., 2019a). In the photogrammetry technique, which is a good alternative to traditional methods in the documentation of cultural heritage, photographs of the object can be obtained, and a 3D model can be generated with the help of certain mathematical models. Ulvi et al. (2019b) conducted a study on the modeling of historical fountains using the close-range photogrammetry method. Yakar and Doğan (2018) examined the use of the SfM method in different study areas and stated that it gives consistent results in archaeological sites. Today, due to the relatively inexpensive and portable nature of

* **Corresponding Author**

*(hsenol@harran.edu.tr) ORCID ID 0000-0003-0235-5764
(nizarpolat@harran.edu.tr) ORCID ID 0000-0002-6061-7796
(yunuskaya@harran.edu.tr) ORCID ID 0000-0003-2319-4998
(akadirm@harran.edu.tr) ORCID ID 0000-0002-9072-869X
(mulukavak@harran.edu.tr) ORCID ID 0000-0003-2092-3075

Research Article / DOI: 10.53093/mephoj.899157

Cite this article

Senol H I, Polat N, Kaya Y, Memduhoglu A & Ulukavak M (2021). Digital documentation of ancient stone carving in Şuayip City. Mersin Photogrammetry Journal, 3(1), 10-14

Received: 03/18/2021; Accepted: 29/05/2021

digital handheld cameras, terrestrial photogrammetry is frequently used in archaeological sites (Ulvi et al., 2019b). Digital handheld cameras used in terrestrial photogrammetry can be calibrated both before and during the task and store the information required for 3D modeling. In this way, 3D models can be obtained with calibrated cameras. By using superimposed photographs with the Structure from Motion (SfM) method, a 3D model of the object can be generated.

The name of the city of Şanlıurfa has become popular not only throughout the country but also throughout the world, thanks to the cultural heritage in the province. Göbeklitepe (Kurt and Göler, 2017), Karahantepe (Çelik, 2011), Harran City (Green, 1992), Soğmatar (Albayrak and Çelik, 2019) and many others are important archaeological sites which attracts the local and foreign tourists. Many archaeological excavations and academic studies have been carried out in these areas from the past to the present. Şenol et al. (2020) used terrestrial laser scanner and drone data to model the Kızılkoyun Rock Tombs. Polat et al. (2020) modeled small objects extracted at the Harran Archaeological Site with the photogrammetry method and transferred them to digital environment in a scaled and precise manner. Şenol et al. (2017) used the terrestrial laser scanning method to model the city of Harran in their study. Ulukavak et al. (2019) modeled the Harran ruins with the photogrammetric method. Although there are studies on the Harran and Göbeklitepe archaeological sites in the province of Şanlıurfa in the literature, there are not many studies on the ancient city of Şuayip, which is the subject of this study.

In this study, the inscription on the wall next to the entrance door of a cave in the ancient city of Şuayip was examined. Unearthing and documenting this inscription, which is an important heritage related to the region, is critical for the continuity of the cultural heritage. Accordingly, in this study, the 3D documentation, automatic drawing and visualization of the inscription engraved on the wall were made.

1.1. Study Area

The ancient settlement known as Şuayip City, which constitutes the study area, is located in the Tektek Mountains approximately 80 km southeast of Şanlıurfa (Figure 1). It is understood that the settlement is spread over a low rocky hill and its skirts.

Although the ancient name of the settlement is not known precisely, there are suggestions regarding it (Sinclair 1990, 189-190; Lipinski, 2000, 124; Güler, 2016, 170). The belief that Prophet Şuayip lived here for a while and the acceptance of one of the rock settlements in the area as the quarter of Prophet Şuayip has resulted in this settlement being called "Şuayip City" today.

Although the buildings in the area are mostly from the Late Antique Era, it is suggested that some of them may have been built in the first century (7th century) of the Arab invasion (Sinclair 1990, 189-190). Two different architectures stand out in the field within the framework of the first observations. These are the spaces carved into the bedrock and the structures made of cut block stones on the bedrock. Besides, the presence of some structures made of cut blocks and stairs leading down to the rooms carved into the bedrock below were found. This shows that rock settlements and structures made of cut blocks are used together and that two different architectural approaches constitute a single structure.

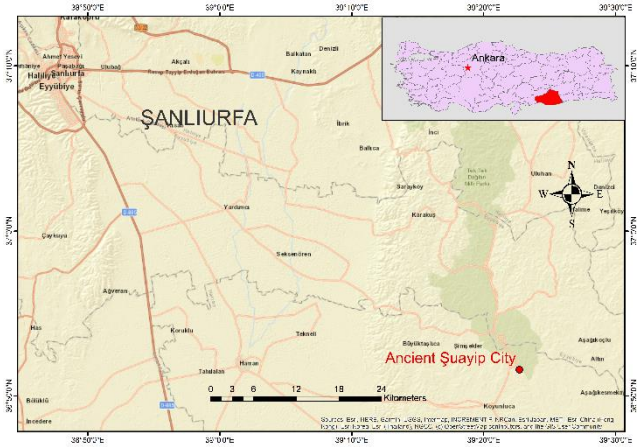

Figure 1. Study area

As seen from the surface remains, the structures made of cut block stones are mainly concentrated on the northern and western slopes of the hill. Some of these structures, which are seen at the level of footing blocks in most of the area or are under the ground, have been preserved until today to give surface architecture. In this study, a carving stone found in the city of Şuayip was examined (Figure 2).

Figure 2. Carving stone

It is observed that the carving stone deforms over time and becomes incomprehensible. For this reason, the deformed area was examined with the photogrammetry technique and the photographs of the carving stone were taken with the terrestrial photogrammetry technique.

1.2. Equipment

Canon 2000D DSLR camera was used in the study (Figure 3). To document the archaeological site using

the terrestrial photogrammetry technique and to obtain a 3D model, it is necessary to take overlapping photographs to cover the entire structure. Information about the digital camera used in the study is given in Table 1.

Figure 3. The camera used in this study

Table 1. Equipment specifications

Feature	2000D Value
Megapixels	24.1
Maximum Image Resolution	6000 x 4000 pixels
Weight	475 g
Size	129 x 101.3 x 77.6 mm
Sensor Size	22.3 x 14.9 mm

2. METHOD

Terrestrial photogrammetry is a method that enables 3D drawings to be made at near and far distances. By using cameras with different focal lengths and special software, necessary orientations are made and 3D models are produced from the photographic surface. With this method, 3D location information of the objects whose models are obtained is created (Şanlıoğlu et al., 2013). Terrestrial photogrammetry is used in many application areas. These areas are preferred in architecture, archeology, industry, land surveys, medicine, criminology, traffic accidents, and many other areas. Thanks to CAD-based software, the application areas of terrestrial photogrammetry are shifting to different areas according to the imagination of the person (Ulvi et al., 2020).

Survey plans, orthophoto, profile extractions, and 3D models obtained from photographs taken from historical buildings are used to document cultural heritage. In this way, it is possible to reconstruct cultural values that may be deformed or damaged over time.

SfM is a photogrammetric method used to create 3D models of a feature or topography from two-dimensional photographs that overlap in many positions and directions to recreate the photographed object (Figure 4).

This technology exists in various forms since 1979, but applications were not common until the early 2000s. SfM technique is a method that can model the object in 3D in the digital environment by using many images of a 3D object taken from different angles. Traditional photographic techniques require precise 3D location and orientation information of cameras and control points for geometric modeling. On the other hand, model geometry, camera position and orientation information can be calculated simultaneously and automatically in the SfM method (Snavely et al., 2008; Önal et al., 2017).

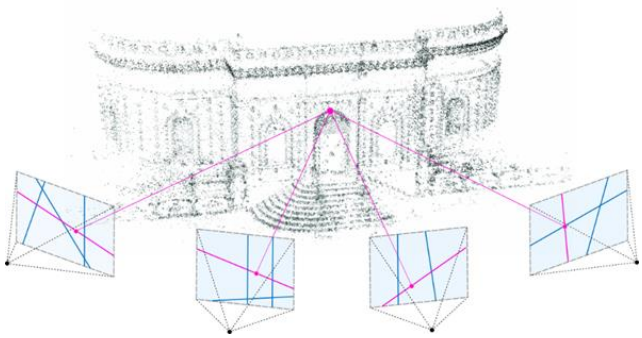

Figure 4. SfM method (Geppert et al., 2020)

SfM's applications range from many geology subfields (geomorphology, tectonics, structural geology, geodesy, mining) to archeology, architecture, and agriculture. In addition to orthorectified images, SfM generates a dense point cloud dataset like those produced by airborne or terrestrial LiDAR.

3. APPLICATION AND RESULTS

For 3D modeling, a total of 42 photographs of the object were taken from different angles. The shooting was done with a Canon 2000D camera. In the SFM technique, since the model geometry and camera position information are resolved simultaneously and automatically, there is no need for camera calibration (Sarıtürk & Şeker, 2017).

Agisoft PhotoScan software is a photo-based modeling program that is often used to produce high-quality 3D models from photographs. In this study, Agisoft PhotoScan software was preferred as commercial software. The photos obtained with the camera were transferred to the software, and a point cloud was created by matching the photos. Approximately 4.6 million points were produced in the model made with the terrestrial photogrammetry technique. The noise-generating points were cleaned and then a dense point cloud was formed. After cleaning the dense point cloud, the solid model was produced, and the 3D model was generated by using the texture information (Figure 5).

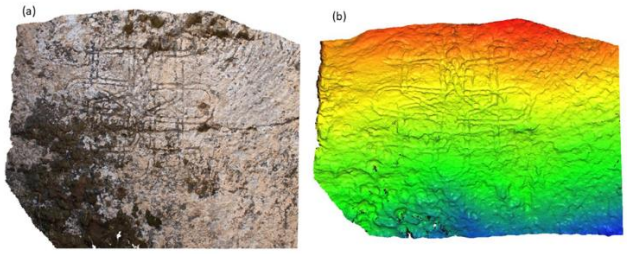

Figure 5. (a) Point cloud and (b) solid model

To reveal the inscription automatically, an elevation model was created first. The inscription was tried to be revealed by the depth through these elevation models (Figure 6).

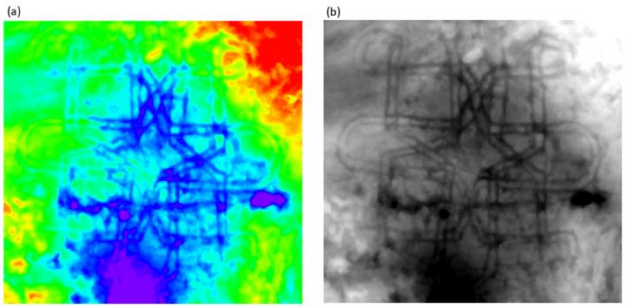

Figure 6. (a) Colored elevation model and (b) elevation model in grayscale

The height model was not sufficient to reveal the entire inscription. Different heights have emerged and inscription depths could not be obtained because of the surface deformation and mosses on the stone. So, the inscription was tried to be extracted by different analysis techniques using verticality, surface variation, directional and Gaussian high pass filters (Figure 7).

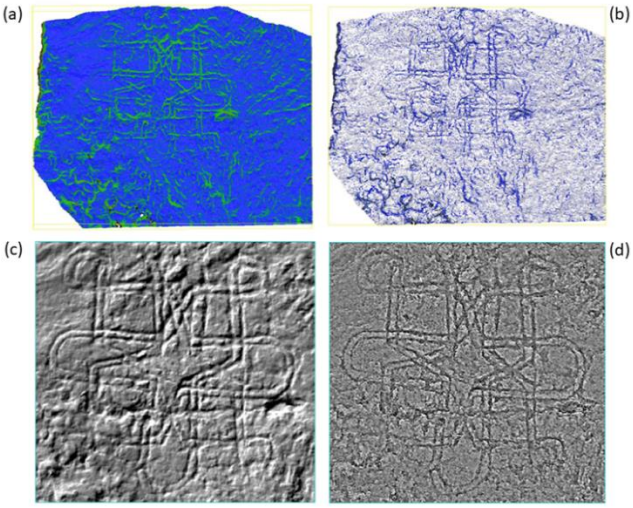

Figure 7. The results of; (a) verticality filter, (b) surface variation filter, (c) directional filter, and (d) Gaussian high pass filter

As seen in figure 7, the results of four different filters present valuable information to define the ancient stone carving. Especially the linear parts of the carving were highly emphasized.

4. CONCLUSION

In this study, the historical carving stone found in the archaeological excavation area of Şuayip city was modeled by photogrammetric methods. The modeling process was done by taking terrestrial photographs of the building. The fact that the surface of the carving stone was deformed too much, and the inscription depth was insufficient has been a struggle for the study. In this direction, first the point cloud and then the 3D model of the area was produced. As a result of the study, approximately 4.6 million points were produced by terrestrial photogrammetry. Although the elevation model was used at first to overcome the struggle encountered in the study, no meaningful result was obtained due to the roughness of the surface. Later, using filters such as verticality, surface variation, directional and Gaussian high pass, the inscription became visible and distinctive in detail. With the carving stone's revealing and detailed modeling, Şuayip Ancient City which is one of Turkey's forgotten cultural heritage has led to the discovery and saving. Although the photogrammetry technique is sufficient for these studies, a solution can be produced by using the laser scanning method in future studies for such a deformed surface.

ACKNOWLEDGMENT

Supported by the Harran University's Research Projects Department, project number 20115.

Author Contribution

The authors' contributions are equal to all phases of the research and the article.

Conflicts of interest:

The authors declare no conflicts of interest.

REFERENCES

Albayrak Y & Çelik B (2019). Soğmatar Çevresi Kaya Mezarları. *Karadeniz Uluslararası Bilimsel Dergi*, (43), 255-261.

Cömert R, Avdan U, & Şenkal E (2012). İnsansız Hava Araçlarının Kullanım Alanları ve Gelecekteki Beklentiler. *IV. Uzaktan Algılama ve Coğrafi Bilgi Sistemleri Sempozyumu (UZAL-CBS 2012)*, 16-19, Zonguldak.

Çelik B (2011). Karahan Tepe: a new cultural centre in the Urfa area in Turkey. *Documenta Praehistorica*, 38, 241-254.

Eskikurt A (2003). Anadolu medeniyetleri ve coğrafya. Doktora tezi. Erişim Adresi: http://dspace.marmara.edu.tr/handle/11424/27726

Geppert M, Larsson V, Speciale P, Schönberger J L, & Pollefeys M (2020). Privacy preserving structure-from-motion. *In European Conference on Computer Vision* (pp. 333-350). Springer, Cham.

Green T M (1992). The City of the Moon God: Religious Traditions of Harran (Vol. 114). *Brill*.

Guler S E (2016). Urfa Tarihinden Sayfalar, *Eyyübiye Bel. Yayınları, Ankara*.

Kaya Y, Yiğit A Y, Ulvi A, & Yakar M (2021). Arkeolojik Alanların Dokümantasyonununda Fotogrametrik Tekniklerinin Doğruluklarının Karşılaştırmalı Analizi: Konya Yunuslar Örneği. *Harita Dergisi*, 165, 57-72.

Kurt A O & Göler M E (2017). Anadolu'da İlk Tapınak: Göbeklitepe. *Cumhuriyet İlahiyat Dergisi*, 21(2), 1107-1138.

Lipinski E (2000). The Aramaeans: Their Ancient History Culture, *Religion*, (Orientalia Lovaniensia Analecta), Peeters.

Önal O, Bozdağ Ö & Ersoy A (2017). İzmir Agorası'ndaki Roma Dönemine Ait Hamam Yapısının SFM Tekniği ile 3 Boyutlu Katı Modelinin Oluşturulması. *6. Tarihi Yapıların Korunması ve Güçlendirilmesi Sempozyumu.*

Polat N, Önal M, Ernst F B, Şenol H İ, Memduhoglu A, Mutlu S, Mutlu S İ, Budan M A, Turgut M & Kara H (2020). Harran Ören Yeri Arkeolojik Kazı Alanınından Çıkarılan Bazı Küçük Arkeolojik Buluntuların Fotogrametrik Olarak 3B Modellenmesi. *Türkiye Fotogrametri Dergisi*, 2(2), 55-59.

Sarıtürk B & Şeker D Z (2017). Sfm Tekniği ile 3b Obje Modellenmesinde Kullanılan Ticari ve Açık-Kaynak Kodlu Yazılımların Karşılaştırılması. *Afyon Kocatepe Üniversitesi Fen Ve Mühendislik Bilimleri Dergisi*, 17(4), 126-131.

Senol H I, Erdogan S, Onal M, Ulukavak M, Memduhoglu A, Mutlu S, Ernst F B & Yilmaz M (2017). 3D Modelıng Of A Bazaar In Ancient Harran City Using Laser Scanning Technique. *International Archives of the Photogrammetry, Remote Sensing & Spatial Information Sciences*, 42.

Sinclair T A (1990). Eastern Turkey: An Architectural and Archaeological Survey, Vol.IV, *The Lindar Press*, Londos, ss. 189-190.

Snavely N, Seitz S M & Szeliski R (2008). Modeling the World from İnternet Photo Collections. *International Journal of Computer Vision* 80, 189-210.

Şanlıoğlu İ, Zeybek M & Karauğuz G (2013). Photogrammetric Survey and 3D Modeling of Ivriz Rock Relief in Late Hittite Er. *Mediterranean Arhaeology and Archaeometry*, Vol. 13, No 2

Şenol H İ, Memduhoglu A & Ulukavak M (2020). Multi instrumental documentation and 3D modelling of an archaeological site: a case study in Kizilkoyun Necropolis Area. *Dicle Üniversitesi Mühendislik Fakültesi Mühendislik Dergisi*, 11(3), 1241-1250.

Tercan E (2017). İnsansız Hava Aracı Kullanılarak Antik Kent ve Tarihi Kervan Yolunun Fotogrametrik Belgelenmesi: Sarıhacılar Örneği. *Mühendislik Bilimleri ve Tasarım Dergisi*, 5(3), 633-642. doi: 10.21923/jesd.315232

Ulukavak M, Memduhoğlu A, Şenol H İ & Polat N (2019). The use of UAV and photogrammetry in digital documentation. *Mersin Photogrammetry Journal*, 1(1), 17-22.

Ulvi A, Yakar M, Yiğit A & Kaya Y (2019). The Use of Photogrammetric Techniques in Documenting Cultural Heritage: The Example of Aksaray Selime Sultan Tomb. *Universal Journal Of Engineering Science*, 7(3), 64-73. doi: 10.13189/ujes.2019.070303

Ulvi A, Yakar M, Yiğit A Y & Kaya Y (2020). İHA ve Yersel Fotogrametrik Teknikler Kullanarak Aksaray Kızıl Kilise'nin 3 Boyutlu Nokta Bulutu ve Modelinin Üretilmesi. *Geomatik Dergisi*, 5(1), 22-30.

Ulvi A, Yiğit A Y & Yakar M (2019). Modeling of Historical Fountains by Using Close-Range Photogrammetric Techniques. *Mersin Photogrammetry Journal,* 1(1), 1-6.

Yakar M & Dogan Y (2018). 3D Reconstruction of Residential Areas with SfM Photogrammetry. *In Conference of the Arabian Journal of Geosciences* (pp. 73-75). Springer, Cham.

Yakar M, Kabadayı A, Yiğit A Y, Çıkıkcı K, Kaya Y & Catin S S (2016). Emir Saltuk Kümbeti Fotogrametrik Rölöve Çalişmasi Ve 3 Boyutlu Modellenmesi. Geomatik, 1(1), 14-18.

Yakar M, Orhan O, Ulvi A, Yiğit A Y & Yüzer M M (2015). Sahip Ata Külliyesi Rölöve Örneği. TMMOB Harita ve Kadastro Mühendisleri Odası, 10.

Mersin Photogrammetry Journal

https://dergipark.org.tr/en/pub/mephoj

e-ISSN 2687-654X

Documenting historic tileworks using smartphone-based photogrammetry

Ali Asadpour *[1]

[1]*Shiraz University of Arts, Faculty of Architecture & Urbanism, Department of Interior Architecture, Shiraz, Iran*

Keywords
Smartphone
Documentation
Photogrammetry
Tile paintings
Ḥāfeẓ tomb

ABSTRACT

Photogrammetry is a metric technique for indirect measurement through images. This technique could be applied in recording architectural features and documenting buildings. Therefore, smartphone-based photogrammetry can be considered a creative method for architects and conservators to document monuments quickly and promptly. The main objective of this paper is to study the smartphone-based photogrammetry capabilities in two case studies in terms of accuracy and precision. Historic tileworks in Ḥāfeẓ tomb, Shiraz, Iran, has been considered as examples of traditional decorations in Iranian architecture. For this purpose, close-range photogrammetry with stereo photography was used. A smartphone camera has captured the photos. Photogrammetric steps were performed in Agisoft Metashape Professional. The result was 3D models and an orthoimage of the tiles. The accuracy of the results was acceptable for ordinary documentation and differed on average 0.45% to as-built measures. Orthoimage is believed to be an important document for analyzing and studying the patterns and colors used in these works of art. The results of this study emphasized that close-range photogrammetry with a smartphone can in the future be a public and reliable technique for documenting architectural heritages, especially in medium and small-scale projects.

1. INTRODUCTION

Documentation is defined as a systematic collecting and archiving activity to prepare historic building records (Stylianidis, 2020). However, it is a costly and time-consuming procedure, particularly in documenting architectural ornaments and interior decorations. Much of these architectural heritages have been disappeared at a higher rate than that which could be well documented in the last decades by the rapid reconstruction or renovation policies. Hence, developing a cheap and easy technique for documentation is necessary. Recording all of these works is difficult and perhaps impossible. Since digital cameras are one of the practical and relatively inexpensive devices for documentation, photogrammetry would be an affordable, instantaneous, and accessible technique to record architectural evidence and documenting as-is features and building properties.

The idea of Single Images in Conservation recommended by International Committee for Architectural Photogrammetry, CIPA, also presupposes the importance of images in the conservation of architectural heritages (see Schuhr & Kanngieser, 1999, 2003). CIPA's general mission also emphasizes the development of principles and practices for recording, documenting, and managing information by specialized tools and techniques (Quintero et al., 2017). It seems that photogrammetry could be a cost-effective method in the future. That means it could be more pervasive than it is today.

Since photogrammetry is a 3D measuring technique through a central projection model, it should be considered as a multidimensional discipline that integrates art, science, and technology. The primary purpose of a photogrammetric measurement is the three-dimensional reconstruction of an object, which can be re-accessed at any time. Another purpose is producing an orthoimage that can be used for real distance measuring, which is being done on maps with the consideration of scale factor since it is adjusted properly for elevation, lens distortion, and camera tilt (Luhmann, Robson, Kyle, & Harley, 2011; Stylianidis, 2020). These features make photogrammetry attractive for experts in the fields of architecture, conservation, archeology, and documenting cultural heritage. In this context, architectural photogrammetry can pave the way for accurate documentation and could be rapidly widespread by the growth of mobile

* **Corresponding Author**

*(asadpour@shirazartu.ac.ir) ORCID ID 0000-0002-6837-0804

Cite this article

Asadpour A (2021). Documenting historic tileworks using smartphone-based photogrammetry. Mersin Photogrammetry Journal, 3(1), 15-20

Research Article / DOI: 10.53093/mephoj.899432

Received: 03/18/2021; Accepted: 05/29/2021

digital camera technology and by the development of photogrammetry applications.

The main objective of this study is to present the accuracy, precision, and ability of a smartphone for architecture photogrammetry. Therefore, a set of tiles, which cannot be easily well documented with ordinary photography due to their dimensions and position, was selected for this survey. These tiles have historical value and should be considered a masterpiece. In the following, the steps of capturing, data processing, generating the final 3D model, and orthoimage production has been described.

2. LITERATURE REVIEW

There are not many published articles about smartphone-based photogrammetry. Available researches could be divided into two categories: The first group is papers that aim to measure the accuracy of smartphone cameras for photogrammetry purposes. The second category is papers that have used smartphone-based photogrammetry for architectural documentation.

Ebrahim (2004) evaluated the use and accuracy of two digital built-in mobile phone cameras in a laboratory and a field test. His results were promising in terms of using smartphone cameras to a certain estimated accuracy of 1/400. The photo resolution of his mobile phone was 640 by 480 pixels. For this reason, he attributed the poor accuracy of mobile cameras to their lack of resolution. Gruen and Akca (2007) calibrated various mobile phones over indoor tests using self-calibration. Despite some diagnosed substantial systematic errors, they stated that if handle properly, these devices could give us a very interesting option doing smartphone-based photogrammetry in terms of accuracy, costs, and flexibility. Takahashi and Chikatsu (2009) conducted the calibration of indoor and outdoor target tests for seventeen smartphones with 10-megapixel cameras. They concluded that mobile phone cameras can take the place of consumer-grade digital cameras. In 2011, Sarhan Satchet compared the mobile cameras with digital cameras in twenty-four targeted test fields; he suggested that whenever mobile camera resolution increases the Root Mean Square Error dwindle. It should not be forgotten that all these mobile phones tested so far had a resolution of 5 to 10 megapixels. One of the most recent studies compared the Nikon D310 camera with two Samsung phones (Note III & S5) and a Sony phone (Xperia Z2) offering 20.7, 16, and 13-megapixel images, respectively. The results of this comparison showed that mobile cameras are efficient, fast, and useful, and their accuracy for close-range photogrammetry is such that it offers good results compared to high-quality cameras. As the quality of the images increases, the desired features in the photogrammetry also improve (Fawzy, 2015).

The effect of the mobile camera quality on improving the accuracy and precision of photogrammetric work in a study by El-Ashmawy (2017) at a university in Cairo has been measured. He tested two 5 and 20-megapixel cameras from one brand. The results showed that higher resolution leads to more accurate results, and in general mobile cameras are suitable for close-range photogrammetry in terms of accuracy, cost, and flexibility. Quite similar results were obtained in 2019 with the test of 5, 8, and 20-megapixel mobile phones revealing that the measurement accuracy in all directions differed only 0.4 to 0.5 mm, which is equivalent to less than half of a pixel (Shatnawi & Obaidat, 2019). In general, these studies show that the higher the resolution of mobile cameras, the better the accuracy of photogrammetry.

Unfortunately, there are very few articles in the field of architectural smartphone photogrammetry. For instance, by a 3D survey of a student design courses model, Hernán-Pérez, Domínguez, González, and Martín (2013) estimated the accuracy of an iPhone based close-range photogrammetry around one centimeter. The findings of the present study could be considered as part of these efforts to develop the use of mobile phones in architectural photogrammetry and documentation of historical monuments.

3. STUDY AREA

The tiles studied in this paper are a part of the Ḥāfeẓ tomb facade, one of the famous Iranian poets of the 14th century, in Shiraz, Iran (Figure 1). Khwāja Shams-ud-Dīn Muḥammad Ḥāfeẓ-e Shīrāzī (1315-1390) lived in Shiraz during Timurid Empire (1370-1507) and died in this city at the age of 74 or 75. Numerous buildings have been established on his grave at different times throughout history, but Karīm Khān-e Zand (1705-1779), founder of the Zand dynasty, built the most significant of them. He installed a marble stone on Ḥāfeẓ grave, established a portico with four columns in front of it, and formed a garden around the tomb in 1772-73, which became the basis for the later developments.

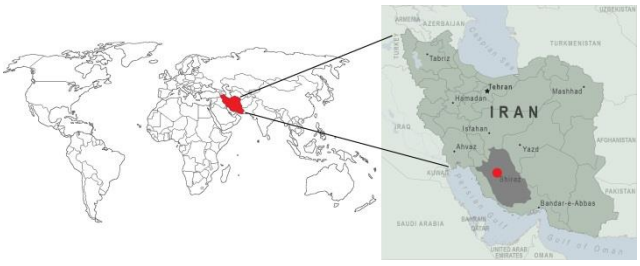

Figure 1. Shiraz location-Fars province/IRAN

In the twentieth century, a French architect and archaeologist, André Godard (1881-1965) was invited to renovate the tomb. Godard developed the Karīm Khān layout, presented a new design, installed a dome with eight columns on the grave and, widened the porch of the Karīm Khān to twenty columns. Designing started in 1936 and the building almost completed in 1938. The tiles of the southern facade of the porch on both the east and west sides are the work of the famous painter of Shiraz, Seyyed Sadr al-Dīn-Shayesteh, and the implementation and installation was done by the famous tile worker of that time, Karim Faghfouri.

This study examined these two 82-year-old tile works on the west and east sides of the central porch

using a smartphone-based photogrammetry procedure. These two tiles are not only located on both sides of the porch but also are symmetrical in design and layout. Figure 2 shows western and eastern tiles. The dimensions of the outer rectangular frame of the western tiles were equal to 2.98 by 4.96 meters. The final height of it is 4.96 meters. The tiles are installed at a height of about 1.50 meters above the pathway. The dimensions of the outer rectangular frame of the eastern tiles were equal to 2.99 by 4.98 meters. The final height of it is 4.98 meters. The location and the height of these tiles make taking flat photos difficult.

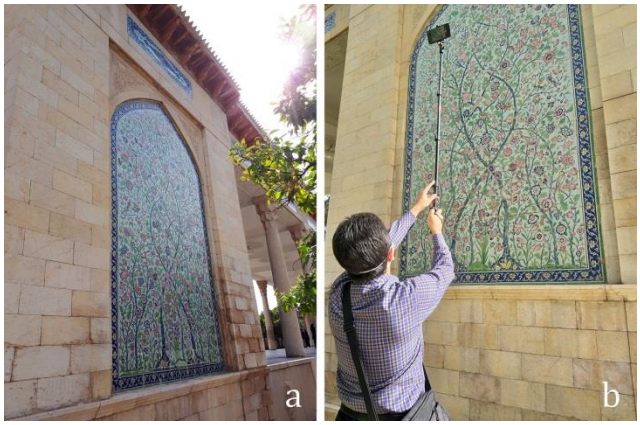

Figure 2. Tiles of the western (a) and eastern parts (b) of the porch in Ḥāfeẓ Tomb

4. METHOD

A Samsung Galaxy A720F/DS (16 MP, f/1.9, and 27 mm) is used for capturing images (Figure 3). All photos were taken with a single camera. To have the highest quality, images were taken in 4608×3456 pixels. On a sunny day in March 2021, shooting was started based on the stereographic principle. The location of the shooting had certain limitations that were part of the study; the pathway in front of the tiles was narrow (about 2 meters) and the trees were an important obstacle for shooting from different distances and stations. For photography, a 1.25 cm long monopod equipped with Bluetooth was used.

Figure 3. Samsung Galaxy A720F and a monopod

An ordinary laser distance meter device on site measured the length and width of these tiles and their outer rectangular stone frame. This device is equipped with a laser grade II, type 635nm with ±3mm accuracy. To ensure the accuracy of the measurements, each distance was measured three times and the value with the highest frequency was used.

This study is based on target-free photogrammetry and its purpose is to show the efficiency and accuracy of smartphone photogrammetry for architectural documentation. However, five checkpoints in each case study were used to assess the accuracy of the orthoimages and scaling the results. These checkpoints are so distributed that they could be identified in both orthoimages and 3D models. Table 1 shows the position of these checkpoints on the facade. Points 1, 2, and 3 are on one plane, and points 4 and 5 are on another plane. Photography started from point 1 and the camera moved in a vertical direction upwards. The same work is done for other parts of the tiles.

Table 1. Five checkpoints distributed on the façade with relevant distances measured on-site

Legend	East Tiles (m)	West Tiles (m)
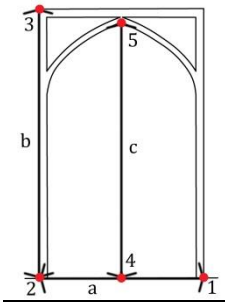	Stone width a=2.984	Stone width a=2.992
	Stone length b=4.960	Stone length b=4.983
	Tileworks length c=4.706	Tileworks length c=4.705

The Agisoft Metashape Professional (2019), as stand-alone automatic lens calibration software, was used for this close-range photogrammetry. The workflow consists of seven consecutive steps:

1- Loading photos into Metashape,
2- Inspecting loaded images, removing unnecessary ones,
3- Aligning photos,
4- Building dense point cloud,
5- Building mesh or 3D polygonal model, 6- generating texture, and
7- Exporting results

Orthoimages were entered in AutoCAD and scaled or checked using on-site measured checkpoints.

5. RESULTS AND DISCUSSION

Eighty-four camera stations (photos) have been used in this project; 39 camera stations for west tiles and 45 stations for east tiles. Because of using a monopod, many of the photos were captured in parallel with the tile works. Due to the height of the tilework and the small distance in front of it, some photos were taken unparalleled. However, efforts were made to avoid oblique photography as much as possible (Figure 4). All photos loaded into the Agisoft Metashape Professional version and aligned successfully. Camera calibrations are reported in Table 2, and image residuals are represented in Figure 5.

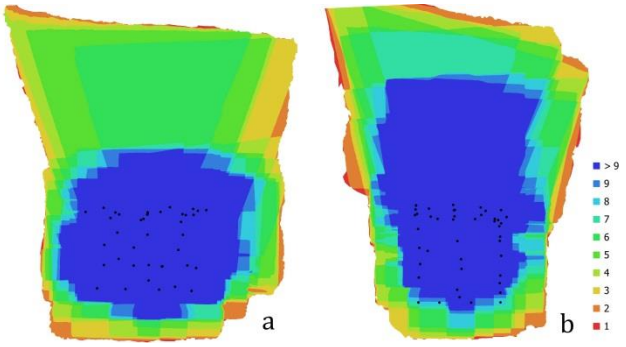

Figure 4. Camera locations and image overlap in West tilework (a) and East tilework (b)

The Samsung Galaxy A720F/DS has a 16-megapixel camera with f/1.9 and a 27mm lens. Thus, a wide range of a scene must be projected on a very small area of the camera sensor. As a result, averaged residuals are not homogenous across the entire surface of the sensor. The wave effect in the error distribution is seen in the image residuals. In the center and peripheral circles, the size of these errors is about 2 pixels, which here equals 2 µm (each pixel was calculated 1 µm in the Agisoft Metashape report). There are more errors in the four corners, especially in the right corners. The wide-angle mobile lens may have exacerbated the errors in the corners. However, the errors are orderly. This concentric distribution of image residuals may be revealing that residuals come from a limited polynomic model. In an inaccurate calibration, these concentric residuals are less conspicuous because, in areas where the projective model does not match the actual behavior of light paths, residuals are much larger (Sanz-Ablanedo, Chandler, Rodríguez-Pérez, & Ordóñez, 2018, p. 8). However, this issue needs more laboratory and field studies.

Table 2. Camera calibration report, Agisoft Metashape

	Items	value	Items	value
West Tiles	F	3659.42 (µm)	k2	-0.595658
	cx	-8.83916 (µm)	k3	0.667333
	cy	37.4567 (µm)	p1	-0.000264763
	k1	0.177442	p2	-0.00105576
East Tiles	F	3714.69458(µm)	k2	-0.647948
	cx	7.11677 (µm)	k3	0.755168
	cy	38.2493 (µm)	p1	-0.000942678
	k1	0.184452	p2	0.000287152

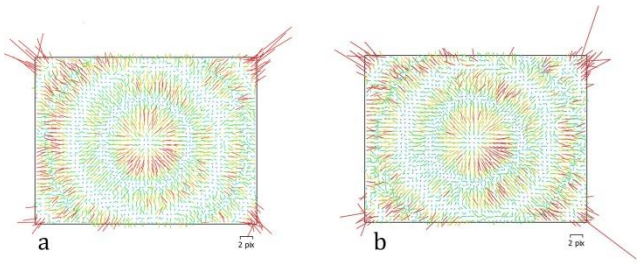

Figure 5. Image residuals for Samsung A720F, West tiles (a) and East tiles (b), Agisoft Metashape Professional report

Building a dense point cloud was the next step in the photogrammetry process (Figure 6). Similarly, the other steps (building mesh and generating texture) were also completed successfully. In the final stage, a three-dimensional model of the tileworks was obtained. This model on the digital platform is exported into 2D orthoimage for further detail drawings. Thanks to the checkpoints measured before, it was possible to scale this 2D image in AutoCAD. To do this, the largest distance measured (parameter (b) according to Table 1) was considered as the basis for scaling. This value was 4.960m and 4.983m for west and east tilework, respectively. As the corners of a stone frame act as checkpoints 2 and 3, these points could be seen well in the orthoimages. Thanks to the accuracy of drawing in AutoCAD, other data could be obtained easily (Figures 7 and 8).

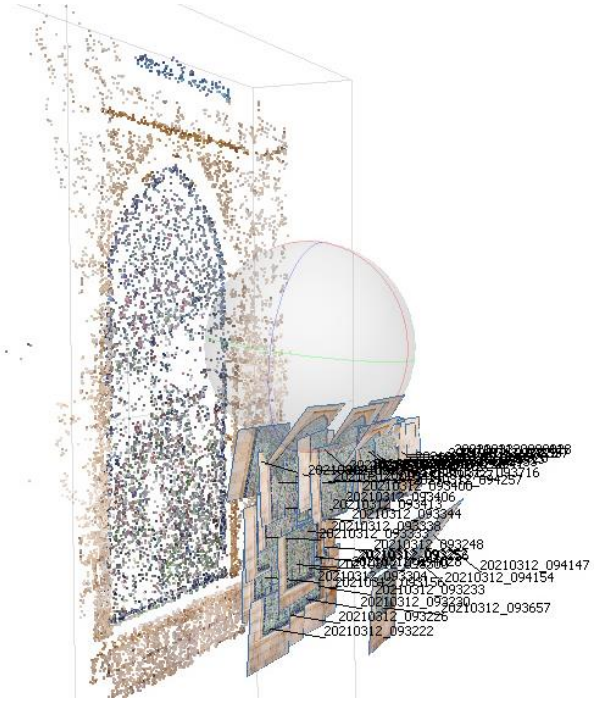

Figure 6. Building point cloud in Agisoft Metashape Professional for west tiles

Comparing the actual sizes with what was measured in the orthoimage shows some differences (Table 3). The maximum difference in dimensions is less than 0.029m, which is equal to less than 1% and the minimum is equal to 0.006m, which is more than 0.1%. In general, it can be said that the average difference in size is equal to 0.45%. Therefore, it could be concluded that the accuracy of the orthoimages is acceptable for architectural ordinary documentation purposes. In addition to the technical structure of the camera and mobile lens, this difference could be due to the low accuracy of the laser distance meter device and the lack of a pre-mounted target on the wall. Accurate detection of checkpoints on the image is associated with errors that can also be effective in the result. To correct this problem, for example, it is possible to install recognizable and measurable targets in place and measure their distances. This job does require more specialized knowledge and skills.

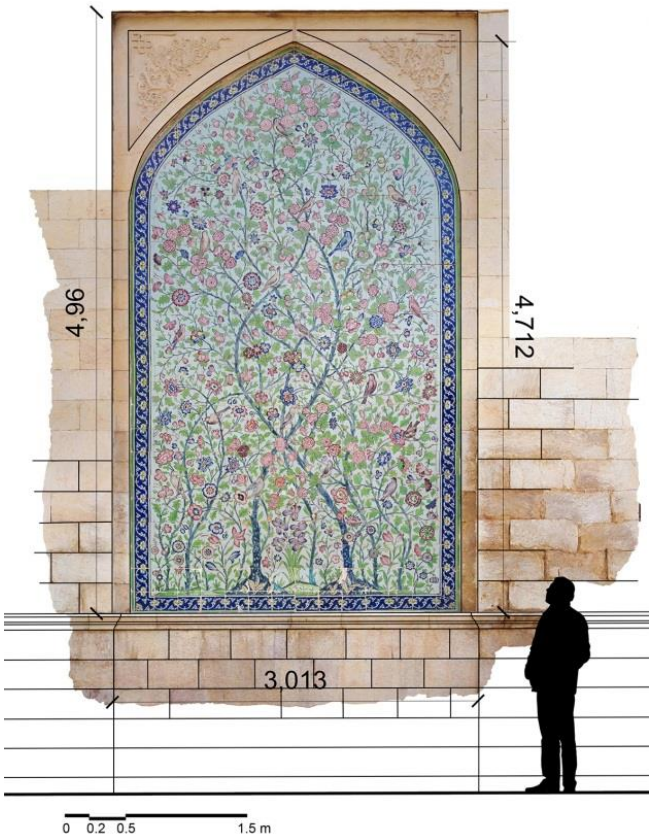

Figure 7. Drawing on the final metric orthoimage of west tilework in AutoCAD

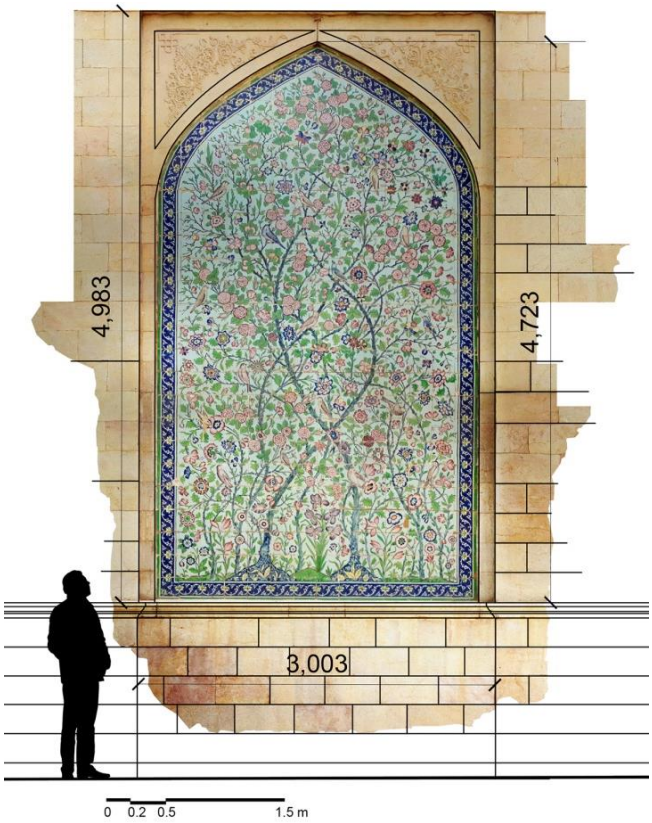

Figure 8. Drawing on the final metric orthoimage of east tilework in AutoCAD

Now that the accuracy and validity of the photogrammetry method and orthoimage production have been confirmed, a final flat image of the west tilework can be obtained (Figure 8). No significant distortion was seen in the orthoimage. Only in the upper section near the arc lines, a slight distortion exists, which may be caused by oblique photography. These distortions had no significant effect on the final quality and visual content of the tiles. The number of photos taken from the top third of the tilework is less than the other sections; maybe having more photos from this part could have reduced or eliminated these distortions in final orthoimage.

Table 3. On-site dimensions and those extracted from orthoimages

	Items	On-site (m)	Orthoimage (m)	Difference (%)
West	Stone width (a)	2.984	3.013	0.97
	Stone length (b)	4.960	4.960	0
	Tileworks length (c)	4.706	4.712	0.12
East	Stone width (a)	2.992	3.003	0.36
	Stone length (b)	4.983	4.983	0
	Tileworks length (c)	4.705	4.723	0.38

Despite all this, the final orthoimage contains the characteristic features of the 82-year-old historical ornaments and records it's actual as-is details. In response to the urgent need of restorers and designers to have exact detailed information, these images could be an important source for conservation, restoration, and repair programs in the future. These digital data can also be used for different types of research in terms of aesthetics, design styles, composition patterns, and the like for those interested in art subjects.

6. CONCLUSION

Documenting monuments and recording buildings ornaments are an essential and even indispensable obligation for all countries, but it can also be very time-consuming and costly. In a country like Iran with an ancient history and diverse cultural heritage, this cannot be done by government or local institutions alone. Universities and NGOs must play an important role in this regard. That is why it is necessary to find cheap and accurate ways and methods for architectural documentation work requiring expertise with cheap and limited equipment.

Today, the mobile phone has become an ordinary and multifunctional device, a cheap and user-friendly tool. Smartphone-based photogrammetry can therefore be an efficient technique for architectural documentation. Working with a smartphone is easier than working with many photogrammetric cameras. It seems smartphone-based photogrammetry has the potential to be further developed in the future. The only challenge is the results accuracy and the degree of its precision.

Smartphone-based photogrammetry can also be considered as part of emergency photogrammetry. In an earthquake-prone country like Iran, where most monuments are made of clay and brick, working with a mobile camera can be an alternative to expensive cameras for small projects. This method can be a quick way with specialized knowledge that can be easily transferred to students or other interested parties.

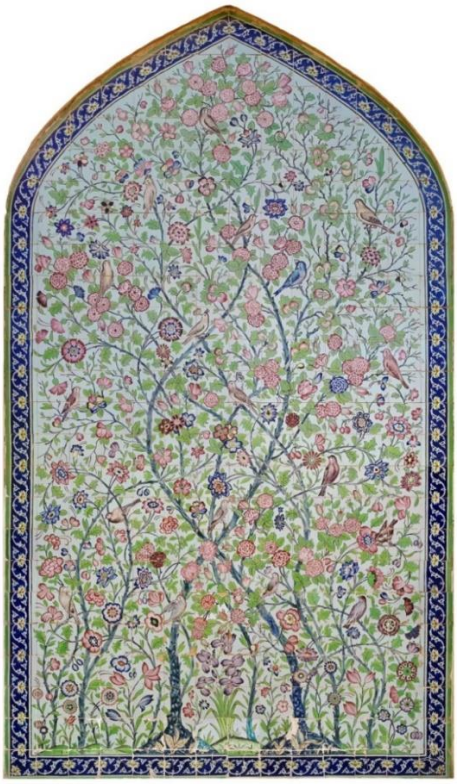

Figure 8. Final orthoimage production of the west tilework

The smartphone-based photogrammetry method is successfully applied in this study. The procedure reliability in terms of accuracy and precision shows acceptable results. On average, about 0.45% discrepancy was calculated in the orthoimage and as-built dimensions measured by laser distance meter. Besides, no significant distortions were observed in the main part of the tileworks. Stereo pair photos, parallel and high-resolution photography can enhance the results. Using mobile phones with higher quality photography and targeting checkpoints in place can increase the accuracy of the work. Laboratory and field studies can further reveal the impact of these suggestions.

The 3D model and the orthoimage obtained from this study are considered part of the digital archive of exquisite tileworks in Ḥāfeẓ tomb, which can be a document and a source for future studies and indirect measurements. The complex layout, colorful design, and diverse elements of these tileworks could not be documented by any conventional or primitive methods. Simple photography could not be useful due to the size of the tiles and their position. Therefore, smartphone-based photogrammetry was a cheap, fast, reliable, and accurate way for our purpose. Further studies could focus on photogrammetry of architectural decorations on curved surfaces or non-flat ornaments like capitals, domes, and the like. The discrepancy between different types of mobile cameras with different brands and resolutions may also be the subject of other researches in smartphone-based photogrammetry.

Conflicts of interest:

The authors declare no conflicts of interest.

REFERENCES

Ebrahim M (2004). Using Mobile Phone Digital Cameras in Digital Close Range Photogrammetry. *The Photogrammetric Journal of Finland, 19*(1), 11-22.

El-Ashmawy K L A (2017). Using smart phones for deformations measurements of structures. *Geodesy and Cartography, 43*(2), 66-72. doi:10.3846/20296991.2017.1330770

Fawzy H E-D (2015). The accuracy of mobile phone camera instead of high resolution camera in digital close range photogrammetry. *International Journal of Civil Engineering and Technology, 6*(1), 76-85.

Gruen A & Akca D (2007). *Mobile Photogrammetry.* Paper presented at the Dreiländertagung SGPBF, DGPF und OVG, „ Muttenz, Switzerland.

Hernán-Pérez A S, Domínguez M G, González C R & Martín A P (2013). Using IPhone Camera in Photomodeler for the 3D Survey of a Sculpture as Practice for Architecture's Students. *Procedia Computer Science, 25*, 345-347. doi:https://doi.org/10.1016/j.procs.2013.11.041

Luhmann T, Robson S, Kyle S & Harley I A (2011). *Close Range Photogrammetry: Principles, Techniques and Applications*. Scotland, UK: Whittles Publishing.

Quintero M S, Georgopoulos A, Stylianidis E, Lerma J L & Remondino F (2017). CIPA's Mission Digitally Documenting Cultural Heritage. *APT Bulletin: The Journal of Preservation Technology, 48*(4), 51-54. Retrieved from https://www-jstor-org.i.ezproxy.nypl.org/stable/26382567

Sanz-Ablanedo E, Chandler J H, Rodríguez-Pérez J R & Ordóñez C (2018). Accuracy of Unmanned Aerial Vehicle (UAV) and SfM Photogrammetry Survey as a Function of the Number and Location of Ground Control Points Used. *Remote Sensing, 10*(10), 1606. Retrieved from https://www.mdpi.com/2072-4292/10/10/1606

Schuhr W & Kanngieser E (1999). *Single images in conservation*. Paper presented at the CIPA Task Group 2; CIPA Symposium Olinda, Brazil.

Schuhr W & Kanngieser E (2003). *New perspectives for single images in conservation*. Paper presented at the CIPA Task Group 2; CIPA Symposium, Antalya, Turkey.

Shatnawi N & Obaidat M T (2019). Extraction of As-Built Drawings Using Cell Phone Camera. *Jordan Journal of Civil Engineering, 13*(1), 21-29.

Stylianidis E (2020). *Photogrammetric Survey for the Recording and Documentation of Historic Buildings*. Switzerland: Springer.

Takahashi Y & Chikatsu H (2009). Accuracy Aspects of Mobile Phone Cameras for Digital Close Range Photogrammetry. *Journal of the Japan society of photogrammetry and remote sensing, 48*(5), 299-307. doi:10.4287/jsprs.48.299

Mersin Photogrammetry Journal

https://dergipark.org.tr/en/pub/mephoj

e-ISSN 2687-654X

Using photogrammetric modeling in reverse engineering applications: Damaged turbocharger example

Engin Kanun[*1]

[1]*Mersin University, Faculty of Engineering, Mechanical Engineering Department, Mersin, Turkey*

Keywords
Mechanical Parts Modeling
Photogrammetry
Reverse Engineering
Turbocharger
3D Modeling

ABSTRACT

Engineering in different areas such as design, manufacture, quality control, research and development, damage analysis, etc. increasingly needs fast, detailed and accurate three-dimensional (3D) documentation of mechanical parts. Moreover, not only in the production and design processes, but also in the post-production stages, the details of the parts may need to be documented in the exact dimensions. Identifying an assembly's components and their interrelationships, producing new digital 2D-3D models of the assembly or parts, rebuilding a part or assembly, examining parts to ensure quality and tolerances, improving performance and if there are any, determining the damaged sections are some of the essential applications of reverse engineering. The purpose of this article is to demonstrate the implementation of a low cost scanning system to create digital copies of mechanical parts. In this study, a mobile phone-based photogrammetric technique is applied to obtain a 3D model of the damaged turbocharger of a car. Firstly, the turbocharger was dismantled into two parts. Both parts were individually modeled and then assembled together. Thus, the turbo wings under the covers were modeled in detail. Accuracy analysis in terms of dimensions was performed in the obtained model. Finally, a simple CFD application was made on a section of the compressor wheel of the turbocharger. Accuracy analyzes of the 3D models showed that less than 0.5 mm accuracy can be obtained without difficulty.

1. INTRODUCTION

In the fields of mechanical engineering and industrial production, reverse engineering (RE) is considered as a method of producing engineering design data and documentation from existing parts and their assemblies (Kumar et al. 2013). The main objective of the RE process, considering engineering applications, is to obtain information from the acquired raw data to recreate a proper parametric CAD model that is as accurate as possible to the object's original design. The composing CAD features are expected to be precise in their dimensions, combinatorial structure and in their current relations (i.e. geometric constraints, symmetries, regularities) between them. Due to the growth and dissemination of 3D scanning technologies and the increasing number of potential applications, the reconstruction of digital geometric models of physical objects, typically referred to as Reverse Engineering (RE) in the field of Computer Aided Design (CAD), has been extensively studied in recent years (Buonamici et al. 2018).

There are plenty of reasons to use RE. The main purpose of selecting RE as a method of development is the absence of a 3D CAD digital model (Dúbravcík and Kender 2012). For parts that have to be duplicated or modified, CAD models are often unavailable or unusable. This is a substantial problem for long life cycle systems for which replacement part inventories have been exhausted and original suppliers are unable or unwilling to provide custom production runs of replacement parts at affordable prices and in a timely manner. Either the CAD systems were not included in the original design or the original design documentation is otherwise insufficient or unreliable for many parts. CAD models, even when they exist, may not be adequate to permit modification or manufacturing using conventional technologies for a number of reasons. Production line alterations to the original design may indicate that the geometry of the component is no longer accurately

* **Corresponding Author**

* (ekanun@mersin.edu.tr) ORCID ID 0000– 0002 – 2369 – 5322

Cite this study

Kanun E (2021). Using photogrammetric modeling in reverse engineering applications: Damaged turbocharger example. Mersin Photogrammetry Journal, 3(1), 21-28

Research Article / DOI: 10.53093/mephoj.901188

Received: 22/03/2021; Accepted: 06/01/2021

represented by the original CAD model. To generate CAD models of a part based on sensed data acquired using three-dimensional (3-D) position digitization techniques, reverse engineering methodologies can be used (Thompson et al. 1999).

Since it usually refers to a product with geometrically complex freeform shapes, measuring and modeling such a component with traditional measurement methods is very difficult (Yılmaz et al. 2008). The use of scanned data in the form of point clouds enables the designer of a machine to produce a detailed CAD 3D model, which can then be used for determining manufacturing quality, CAE system-based redesigning, engineering and simulation tests, and many more (Deja et al. 2019).

Reverse engineering is utilized in engineering, medical sciences, restoration processes for the conservation of cultural heritage, automotive industry, shipbuilding industry etc. (Yılmaz et al. 2000; Verim and Yumurtacı 2020; Dúbravcík and Kender 2012; Deja et al. 2019).

When mechanical engineering applications are taken into consideration, the essential aim of the reverse engineering is to generate a 3D parametric solid model, which is the most appropriate to the original of the object, by utilizing raw data received from a 3D scanner (Verim and Yumurtacı 2020). Shape engineering, placed at the interface of mechanical engineering, modern geometry, computer science, and statistics, is concerned with the study of mechanical parts and assemblies' geometric properties (Anwer and Mathieu 2016). As an example, the proper functioning of mechanical parts frequently depends on the geometric interrelations between functional surfaces or properties (e.g. parallelism between two planes, orthogonality between axes, etc.) and their repair is essential in most cases (Buonamici et al. 2018).

In the documentation process, photogrammetry is a stand-alone tool (Unal et al. 2004; Ulvi et al. 2019). This method relies on at least two images with overlapping data to ensure that the triangulation process is effective (Yakar and Yılmaz, 2008). The aim of digital close-range photogrammetry is to simplify and accelerate the data recording and processing (Doğan and Yakar 2018).

In this study, mobile phone-based photogrammetry which is a fast, cost-efficient and easy to use method was utilized for 3D model construction.

In the first part of the study, the photographs of the model were taken during the photogrammetric model creation process. Point cloud was obtained in ContextCapture software from the photos taken later. The obtained point cloud was transferred to Agisoft Metashape software and data filtering process was applied. Finally, the 3D solid model was created and accuracy analysis of the obtained 3D model was completed.

The second step of the study includes surface and damage analysis of the turbocharger. The obtained 3D model of the turbocharger had been investigated in terms of stresses and strains by using Ansys Static Structural module.

This paper provides a RE approach to obtain the initial design specifications of mechanical parts and affirms an inspection procedure for them to ensure their consistent performance in the second lifecycle by utilizing mobile phone-based photogrammetric techniques. It also provides an approach to assist the progress of remanufacturing, rebuilding, repairing, modificating, improving etc..

2. METHOD

In this paper, mobile phone-based photogrammetric survey was implemented to obtain the 3D model of the turbocharger which is examined in this study. The damaged turbocharger was dismantled from a 2004 Ford Fusion TDCi car.

Figure 1. Damaged turbocharger of 2004 Ford Fusion TDCi – separated into components

This study consists of two phases such as field work and office work. During the field work, photogrammetric images were captured with the aim of obtaining the 3D model of the turbocharger. Digital images of the turbocharger were acquired by using Samsung Galaxy S10 mobile phone. The mobile phone has three rear cameras. The main camera of the phone has 12-megapixels with a 5.6x4.2 mm sensor size. Auto-focusing and focusing at infinity settings were applied. The minimum focusing distance of the camera is 0.10 m and the hyperfocal distance of the camera is 3.60 m. The lens of the camera has a focal length of 4.32 mm and (f/1.5) aperture. Focal length (35 mm eq.) is 27.7714 mm. In addition, the lens has a 66.3° horizontal field of view and 52.2° vertical field of view. Magnification factor was 1x for all photos taken. In addition to all these, camera calibration was performed and the calibration coefficients of the camera were calculated.

First step of the field work was separating the turbocharger into its components for the purpose of creating the detailed 3D model of the components such as turbo-housing, turbo wings of inlet and outlet sides, the main cover etc. After the separation step, camera calibration was completed. A constant focal length during the acquisition and a constant and homogeneous lighting were utilized as much as possible. Blurry photos, flash

light, optical stabilization, digital zoom, and fish-eye lenses were avoided in order to produce better results. With these adjustments, a total of 600 images of the turbocharger were taken.

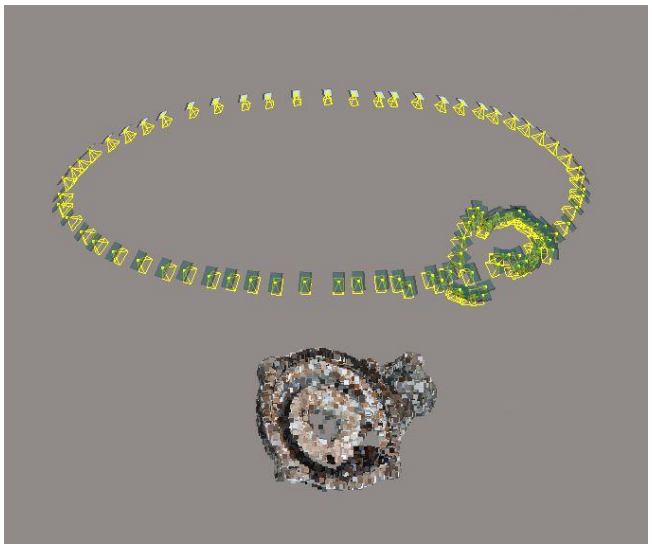

Figure 2. Camera stations configuration of turbo-housing (inside)

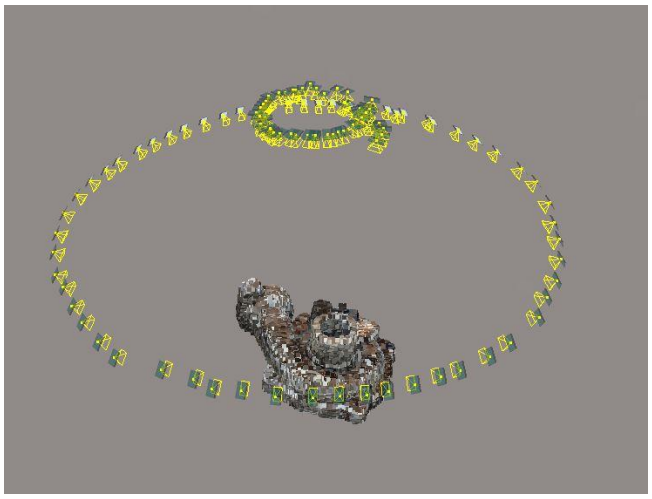

Figure 3. Camera stations configuration of turbo-housing (outside)

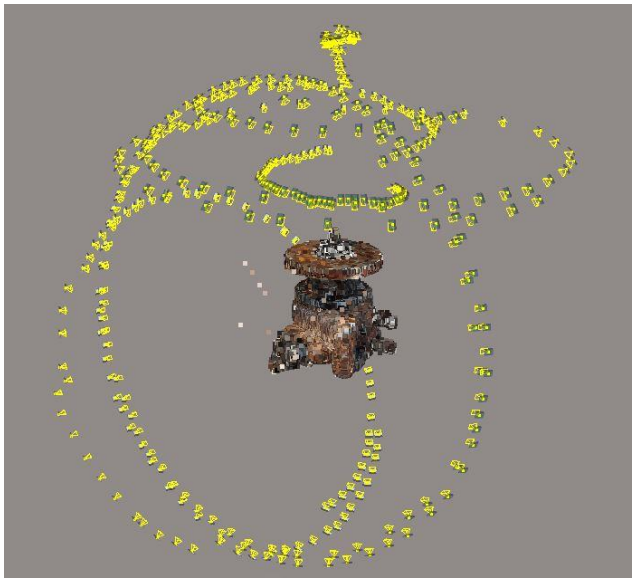

Figure 4. Camera stations configuration of main component and inlet-outlet sides

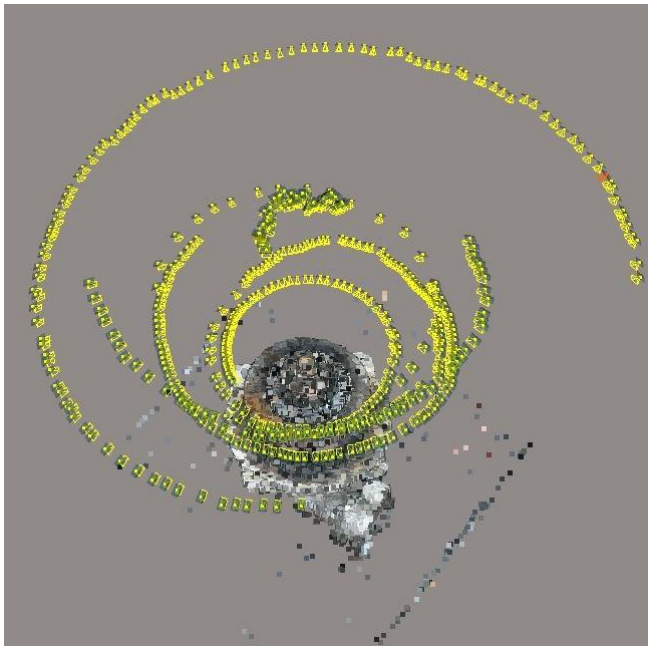

Figure 5. Camera stations configuration of turbine (exhaust-side)

After the completion of the field work, the office work phase was initiated. During the office phase of the study, 599 of the images were processed at Bentley's ContextCapture Software.

Two user tie points were marked on every component of the turbocharger to submit an accurate triangulation to the photos. Then, by taking precise measurements on the parts of the turbocharger, predefined positioning and scale constrains were generated with two user tie points that marked before. Generic block type option was selected with the aim of helping the triangulation process. 'Keep camera calibration' option was selected for aerotriangulation process.

Figure 6. User tie points and scale constrains of the main component

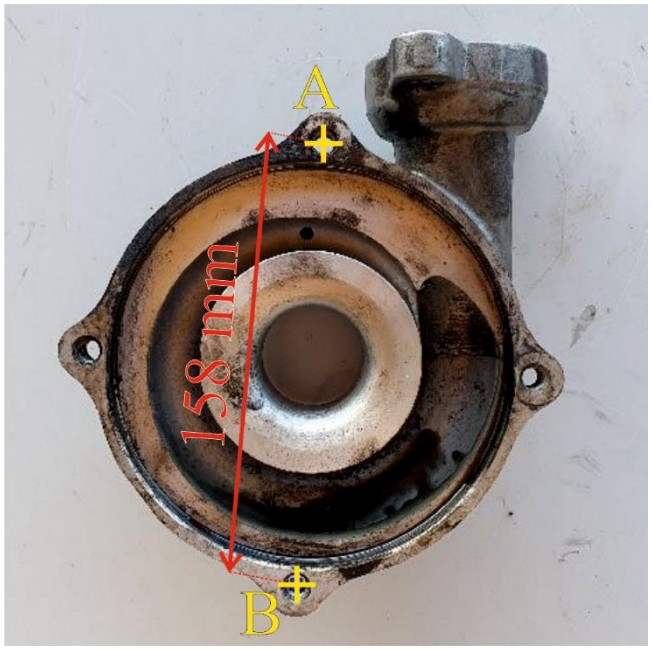

Figure 7. User tie points and scale constrains of the turbo-housing (inside)

Figure 8. User tie points and scale constrains of the turbo-housing (outside)

After the aerotriangulation process, 3D point cloud data generation step was initiated. Colored point cloud was constructed by selecting the options of 1 pixels point sampling, no-compression, and visible colors for color source. The obtained 3D point cloud data was exported to Agisoft Metashape Professional in order to delete redundant points in the data-set and construct an accurate 3D solid model of the turbocharger components.

During the mesh building process, source data was selected as dense cloud which was imported from ContextCapture. Surface type was selected as arbitrary (3D) and high quality face count was applied. Interpolation was enabled and calculate vertex colors option was marked. 9,332,172 points for top turbo-housing, 15,435,364 points for turbo inlet wings, 49,496,656 points for main turbo part, 32,181,638 points for turbine wheel were processed to obtain the 3D solid models.

Figure 9. Turbo-housing dense point cloud obtained by ContextCapture

Figure 10. Main component - dense point cloud obtained by ContextCapture

Figure 11. 3D solid model of turbo-housing obtained by Agisoft Metashape

Figure 12. 3D solid model of main component obtained by Agisoft Metashape

Figure 13. 3D solid model of exhaust outlet wheel obtained by Agisoft Metashape

After the 3D solid model of the turbocharger constructed, accuracy assessment was also implemented. Firstly, a stereolithographic (STL) format of the 3D model was generated to utilize it in ANSYS analysis after accuracy assessment step. With the aim of defining the metric performance of the 3D model, 5 distances between selected detail points on each turbocharger components were compared with the distances acquired from Agisoft Metashape dimensions on each 3D model.

After mesh building and accuracy assessment phases, the mesh files were exported into Rhinoceros 6 software. In Mesh2Surface module, the exact surface models of the obtained meshes were created. Then, surface continuity analyzes of each model were processed to know whether if there was any surface discontinuity or not. The next step contains Fluent analysis of a section of the compressor of the turbocharger in ANSYS 2019 software. The turbo-wing model, compressor-side , were extracted from the main 3D model and were exported into ANSYS Fluent software.

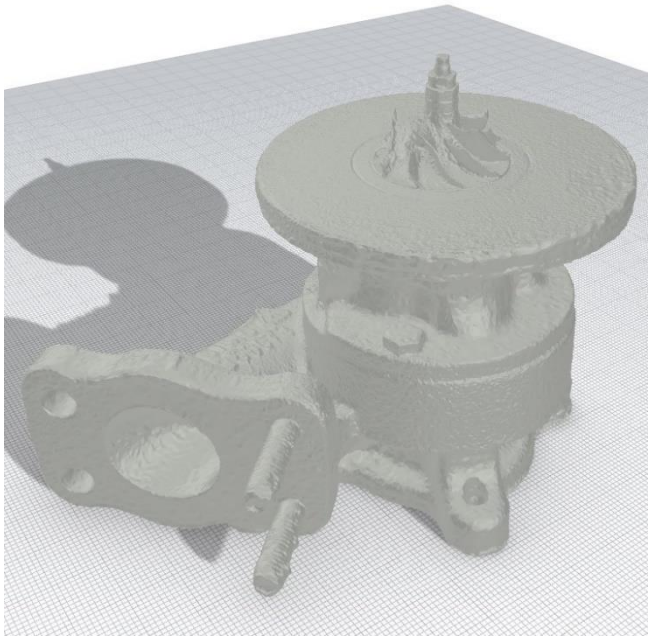

Figure 14. Stereolithographic (STL) format of the 3D model

Figure 15. Detail measurements for accuracy assessment (Exhaust-side, turbine)

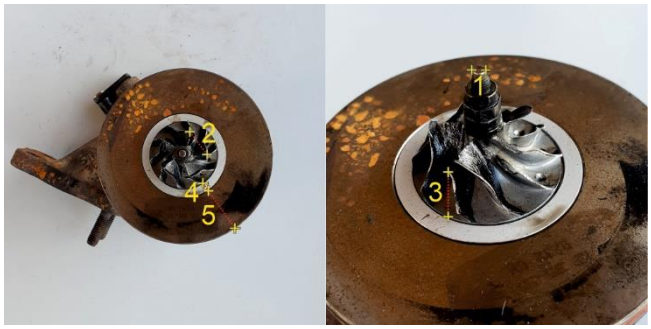

Figure 16. Detail measurements for accuracy assessment (Air-side, compressor)

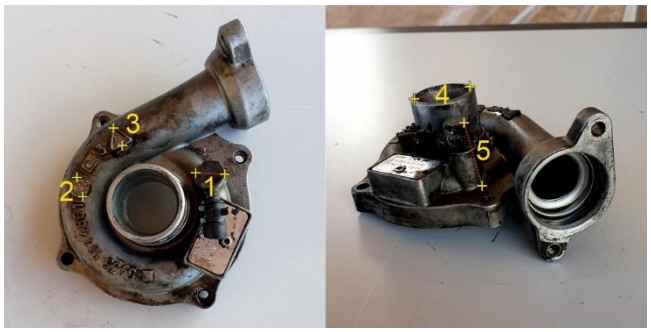

Figure 17. Detail measurements for accuracy assessment (Compressor housing)

Figure 18. Detail measurements for accuracy assessment (Turbine housing)

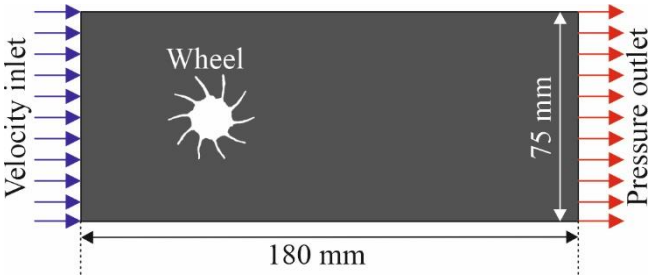

Figure 19. Domain created for Fluent analysis

Subsequently, a random horizontal section was taken from the compressor wheel. Then, it was imported into Fluent software and the domain was created as shown in "Fig. 19" above. After the geometry of the flow area has been created, meshing module was started to generate a mesh. Refinement and inflation were applied around the wheel. In addition, the mesh around the wheel has been densified. According to Bouaifi (2018), ''Close to the wall, there is a thin sublayer with predominantly molecular diffusion. The sublayer has a substantial influence upon the remaining part of the flow. An adequate numerical resolution of a solution in the sublayer requires a very fine mesh because of sublayer thinness and high gradients of the solution.'' Linear element order and 0,005 m element size were applied. Growth rate of 1.2 and defeature size of 2.5e-005 m were decided to generate the mesh. Around the wheel, transition ratio of 0.272 and 2 maximum layers were selected in order to acquire smooth transition.

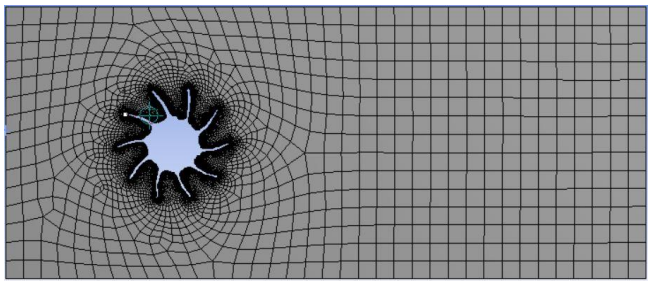

Figure 20. Domain created for Fluent analysis

After mesh generation, flow model options have been set. In calculations, double precision and serial processing were applied. Pressure-based solver, absolute velocity formulation, steady time and planar 2D space were chosen in general settings. K-epsilon (2 eqn.) viscous model was selected. Air was selected as flow material which has an inlet velocity of 5 m/s. Coupled scheme was selected as solution method. Least squares cell based option was selected as gradient. For pressure and momentum, second order terms options were selected. For turbulent kinetic energy and turbulent dissipation rate, first order upwind options were selected. All other settings of the software were left default.

3. RESULTS AND DISCUSSION

Considering the significance of design verification in the overall reverse engineering phase, few, if any, publications on part-to-CAD reverse engineering discuss modeling accuracy (Ingle 1994). After 3D models of the turbocharger were obtained, the accuracy assessment was also completed. The results of the accuracy analyzes were shown in the "Table 1-2-3-4".

Table 1. Exhaust-side turbine model [in mm]

Length	Real	Model	V	VV
1	9.5	9.08	0.42	0.176
2	6	5.92	0.08	0.006
3	6.5	6.21	0.29	0.084
4	5.5	5.13	0.37	0.137
5	12	11.65	0.35	0.123
			RMSE	**0.324**

Table 2. Suction-side compressor model [in mm]

Length	Real	Model	V	VV
1	3	2.99	0.01	0.000
2	15	14.82	0.18	0.032
3	7.5	8.03	0.53	0.281
4	4	4.24	0.24	0.058
5	25	24.72	0.28	0.078
			RMSE	**0.300**

Table 3. Compressor housing model [in mm]

Length	Real	Model	V	VV
1	13.5	13.33	0.17	0.029
2	9.7	10.03	0.33	0.109
3	10	10.09	0.09	0.008
4	31	30.99	0.01	0.000
5	34.5	35.15	0.65	0.422
			RMSE	**0.337**

Table 4. Turbine housing model [in mm]

Length	Real	Model	V	VV
1	28	27.2	0.8	0.640
2	32.5	32.23	0.27	0.073
3	22	22.81	0.81	0.656
4	8	7.75	0.25	0.063
5	25	25.6	0.6	0.360
			RMSE	**0.599**

According to "Table 1-2-3-4", the 3D model of the turbine wheel has a root mean square error (RMSE) of 0.324 mm. The compressor's 3D model has RMSE of 0.300 mm. As for the compressor and turbine housings' 3D models, they have RMSEs of 0.337 mm and 0.599 mm respectively.

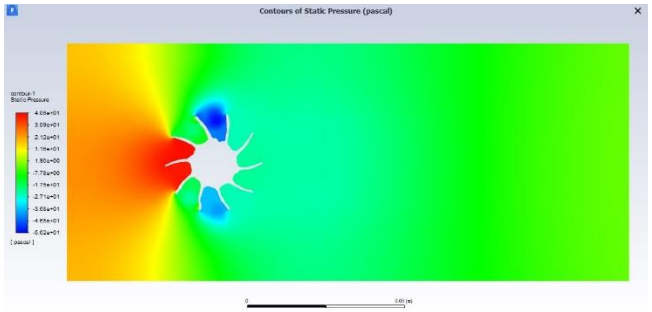

Figure 21. Contours of static pressure (in pascal)

"Fig. 21" indicates the static pressure distribution of the flow domain. Static pressure takes higher values on the inlet side of the wheel. This situation stems from that the wheel decelerates the flow as a barrier. Pressure and velocity are inversely proportional to each other. If pressure increases, the velocity decreases to keep the algebraic sum of potential energy, kinetic energy, and pressure constant. The opposite circumstance is valid for the blue (lower) values on the domain. Where the blue areas started, flow separations occurred and the flow accelerated towards the wheel.

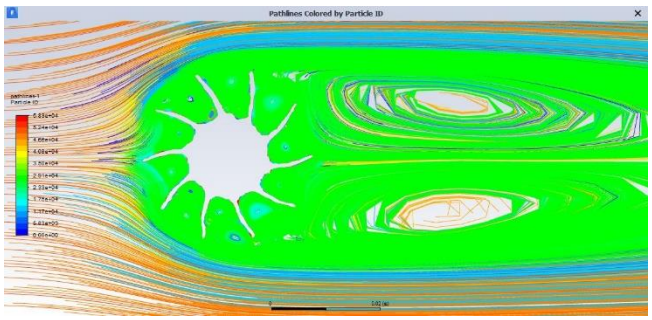

Figure 22. Colored pathlines around the wheel

"Fig. 22" shows the colored pathlines around the wheel. The flow pattern in which fluid particles move irregularly due to flow velocity or surface shape is called turbulent flow (eddy flow). As seen above, many flow irregularities are observed around the wheel. This circumstance was derived from the sharp ends of the wheel. Sharp ends disrupt the continuity of the flow. Streamlines intersect each other, particles mingle with each other, creating a turbulent flow.

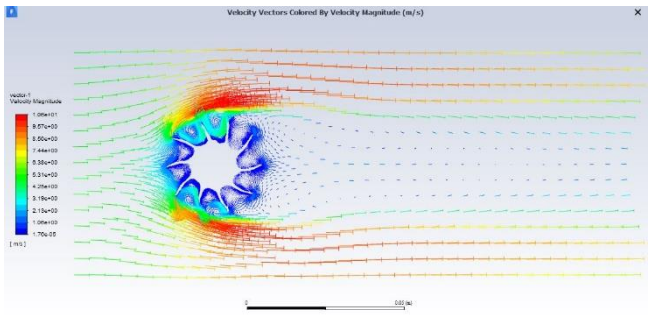

Figure 23. Velocity vectors of the flow domain

"Fig. 23" indicates the velocity vectors of the domain. Higher velocity magnitudes (in m/s) are represented by the color red, while lower values are represented by the color blue. Vector distribution around the wheel shows that the velocity magnitudes take lower values between the wings. Subsequent to the sharp ends of the wheel, speed values increase due to sudden pressure drop. Velocity vectors change direction also.

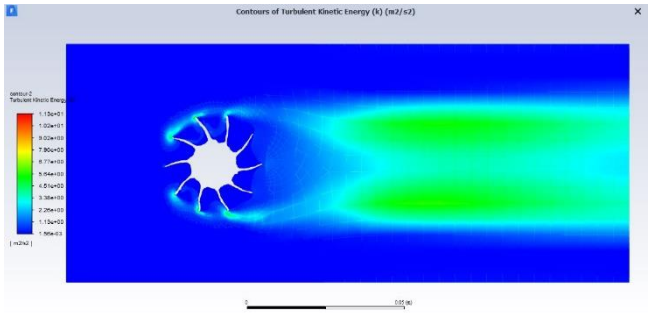

Figure 24. Contours of turbulent kinetic energy (k)

"Fig. 24" demonstrates the contours of turbulent kinetic energy (k) in m^2/s^2. Simply, turbulence is not observed from the inlet area to the wheel. With distortion of streamlines at sharp ends, turbulences occurred and turbulent kinetic energy (k) increased.

Table 5. Moments on the wheel [in N.m]

Zone	Pressure	Viscous	Total
Wheel	-0.1612	0.0015	**-0.1597**

The moment values that the cross section is exposed to is shown in the "Table 5". From the values above, viscous/pressure moments ratio is calculated as 0.93%.

4. CONCLUSION

There are many reasons to use reverse engineering. One of the essential purpose of selecting RE as an engineering calculation method is the deficiency of 3D CAD models of the existing parts. As a result of conducting this research, it is clear to be seen that accurate 3D CAD models of existing machine parts and their engineering calculations can be created/made by using mobile photogrammetric surveys and common engineering softwares. In this research, a damaged turbocharger of a car was separated into its parts and 3D CAD models of each part were acquired. Then, a basic flow calculation around the compressor wheel of the turbocharger was carried out by extracting a 2D section of the compressor.

The findings that are presented in this study suggest that mobile photogrammetric methods provide fast, detailed and accurate 3D documentation of mechanical parts. Accuracy analyzes of the 3D models showed that less than 0.5 mm accuracy can be obtained without difficulty.

This study also indicates that many engineering calculations can be made using 3D models of the mechanical parts.

All things considered, mobile photogrammetric survey is an effective, easy-to-use and accurate method for reverse engineering calculations.

In future studies, handheld laser scanners can be utilized to obtain 3D models of mechanical parts, and can be compared to the mobile photogrammetric results to become aware of which method is more suitable in 3D modeling of mechanical parts.

ACKNOWLEDGEMENT

The author gratefully appreciates the sincere thanks to the Geomatics Engineering Department of Mersin University for their support and contributions to the development of this work.

Conflicts of interest:

The authors declare no conflicts of interest.

REFERENCES

Anwer N & Mathieu L (2016). From reverse engineering to shape engineering in mechanical design. CIRP Annals - Manufacturing Technology, 65(1), 165–168. https://doi.org/10.1016/j.cirp.2016.04.052

Bouaifi M (2018, February 6). Re: Why do we need Finer Mesh near the Wall? Mathematical Reason? [Discussion post]. Researchgate. https://www.researchgate.net/post/Why-do-we-need-Finer-Mesh-near-the-Wall-Mathematical-Reason

Buonamici F, Carfagni M, Furferi R, Governi L, Lapini A & Volpe Y (2018). Reverse engineering of mechanical parts: A template-based approach. Journal of Computational Design and Engineering, 5(2), 145–159. https://doi.org/10.1016/j.jcde.2017.11.009

Deja M, Dobrzyński M & Rymkiewicz M (2019). Application of Reverse Engineering Technology in Part Design for Shipbuilding Industry. Polish Maritime Research, 26(2), 126–133. https://doi.org/10.2478/pomr-2019-0032

Doğan Y & Yakar M (2018). Gis and Three-Dimensional Modeling for Cultural Heritages. International Journal of Engineering and Geosciences, 50–55. https://doi.org/10.26833/ijeg.378257

Dúbravčík M & Kender Š (2012). Application of reverse engineering techniques in mechanics system services. Procedia Engineering, 48, 96–104. https://doi.org/10.1016/j.proeng.2012.09.491

K A Ingle, Reverse Engineering. New York: McGraw-Hill, 1994.

Kumar A, Jain P K & Pathak P M (2013). Reverse engineering in product manufacturing: an overview. Daaam International Scientific Book, 2013. p. 665-678.

Thompson W B, Owen J C, De St. Germain H J, Stark S R & Henderson T C (1999). Feature-based reverse engineering of mechanical parts. IEEE Transactions on Robotics and Automation, 15(1), 57–66. https://doi.org/10.1109/70.744602

Ulvi A, Yakar M, Yiğit A & Kaya Y (2019). The Use of Photogrammetric Techniques in Documenting Cultural Heritage: The Example of Aksaray Selime Sultan Tomb. *Universal Journal Of Engineering Science*, *7*(3), 64-73.

Unal M, Yakar M, Yildiz F (2004). Discontinuity surface roughness measurement techniques and the evaluation of digital photogrammetric method. In: Proceedings of the 20th international congress for photogrammetry and remote sensing, ISPRS, 1103–1108

Verim Ö & Yumurtacı M (2020). Application of reverse engineering approach on a damaged mechanical part. International Advanced Researches and Engineering Journal, 4(1), 21–28. https://doi.org/10.35860/iarej.687014

Yakar M & Yılmaz H M (2008). Kültürel Miraslardan Tarihi Horozluhan'ın Fotogrametrik Rölöve Çalışması ve 3 Boyutlu Modellenmesi. *Selçuk Üniversitesi Mühendislik, Bilim ve Teknoloji Dergisi*, *23*(2), 25-33.

Yılmaz H M, Karabork H, Yakar M (2000). Yersel Fotogrametrinin Kullanım Alanları, Nigde Universitesi Muhendislik Bilimleri Dergisi, 4(1), 18-28.

Yilmaz H M, Yakar M & Yildiz F (2008). Digital photogrammetry in obtaining of 3D model data of irregular small objects. *The International Archives of the Photogrammetry, Remote Sensing and Spatial Information Sciences*, *37*, 125-130.

Mersin Photogrammetry Journal
https://dergipark.org.tr/en/pub/mephoj
e-ISSN 2687-654X

Photogrammetric analysis of multispectral and thermal close-range images

Özgün Akçay[*1]

[1] *Canakkale Onsekiz Mart University, Faculty of Engineering, Department of Geomatics Engineering, Canakkale, Turkey*

Keywords
Photogrammetry
Remote sensing
Multispectral images
Thermal images
Close-range

ABSTRACT

Sensors capable of multispectral and thermal imaging beyond visible bands offer many analysis possibilities for environmental monitoring. Different sensor images constitute an important source of information especially in the fields of agriculture, forestry, geology and energy. Photogrammetric studies have been affected by this development in recent years and have been used in the production of multispectral and thermal models besides the RGB model. However, due to geometric and radiometric resolution differences, it is difficult to combine or evaluate models produced from different types of sensors. In this study, the three-dimensional test field images obtained with RGB, multispectral and thermal sensors were oriented and modeled photogrammetrically. The accuracies of the control points on the produced models were compared and discussed. When the results are examined, control point accuracy was obtained as almost similar as in the RGB model after the orientation based on automatic feature matching. Automatic feature detection and matching in thermal images were not robustly produced due to low geometric resolution. For this reason, manual measurements were performed in thermal images, and the photogrammetric orientation and adjustment process was done accordingly. The fused evaluation approach considering RGB, multispectral and thermal images in one photogrammetric model was also implemented and discussed.

1. INTRODUCTION

Recently, multi-sensor modeling and analyzes have been carried out with terrestrial and UAV-based close-range photogrammetry. Although multispectral and thermal lightweight cameras are relatively low resolution compared to RGB cameras, photogrammetric products three-dimensional models and orthophotos have been considered for monitoring and inspection in many areas such as forestry, agriculture and archaeology.

Studies using multispectral camera images have been involved in photogrammetric processes, especially in agriculture and forestry. Nebiker et al. (2008) presented investigations using low-weight and low-cost multispectral sensors in combination with mini and micro UAVs for remote sensing applications in agricultural test fields. A fully automated digital multispeetral and high resolution image acquisition and 3D-processing system was proposed by Wewel et al., (2014). The multispectral data were processed with a photogrammetric pipeline to create triband orthoimages to extract some Vegetation Indices (VI) such as the Normalized Difference Vegetation Index (NDVI), the Green Normalized Difference Vegetation Index (GNDVI), and the Soil Adjusted Vegetation Index (SAVI), examining the vegetation vigor for each crop (Candiago et al., 2015). Saura et al. (2019) also analysed a vineyard with UAV based multispectral imagery and produced the Digital Elevation Model and NDVI to collect information about the agricultural production such as moisture and biomass density. Minařík and Langhammer (2016) proposed a methodology for assessment of spatial and qualitative aspects of forest disturbance based on the multispectral sensor Tetracam camera with the UAV photogrammetry. Sankey et al. (2021) demonstrated that a model incorporating the fusion of UAV multispectral and structure-from-motion photogrammetry classifies plant functional types and bare soil cover with an overall accuracy of 95% in rangelands degraded by shrub encroachment and disturbed by fire. Xu et al. (2020) acquired high spatial resolution multispectral and RGB imagery over a

* **Corresponding Author**

*(akcay@comu.edu.tr) ORCID ID 0000-0003-0474-7518

Cite this article

Akcay O (2021). Photogrammetric analysis of multispectral and thermal close-range images. Mersin Photogrammetry Journal, 3(1), 29-36

Research Article / DOI: 10.53093/mephoj.919916

Received: 18/04/2021; Accepted: 01/06/2021

subtropical natural forest in southwest China using a fixed-wing UAV system and derived 3D point cloud.

On the other hand, photogrammetric studies which consider both RGB and thermal images are found in the literature. Ribeiro-Gomes et al. (2017) evaluated the use of the Wallis filter for improving the quality of the thermal photogrammetry process using structure from motion software. Despite the low resolution of the thermal imagery compared to RGB imagery, forest structural elements were extracted using both point clouds (Webster et al. 2018). Van der Sluijs et al. (2018) revealed the morphology and daily to annual dynamics of thaw-driven mass wasting phenomenon using photogrammetric terrain models and orthomosaic time series. Zefri et al. (2018) studied about the use of thermal and visual imagery taken by UAV in the inspection of photovoltaic installations. Biass et al. (2019) provided detail in characterizing the emplacement of a compound pāhoehoe lava flow using SfM photogrammetry techniques to visible and thermal data sets. Zumr et al. (2020) utilized a combination of electrical resistivity tomography, close range photogrammetry, and unmanned aerial vehicle (UAV) thermal imaging techniques to detect specific superficial and internal structures of a historical earth-filled dam. A low-cost method was proposed to monitor Stromboli, a volcano in the Aeolian Islands of Italy using a unique 3D thermal photogrammetric modelling workflow. The data acquisition and processing part of this workflow has been tested on Stromboli, a volcano in the Aeolian Islands of Italy (Wakeford et al., 2020).

Studies in which multispectral and thermal three-dimensional photogrammetric models and their analysis are performed together can also be found in the literature. Erenoglu et al. (2017) developed a novel methodology extracting and distinguishing material features from UAS-based multi-sensor data photogrammetry for the cultural heritages. Edelman (2018) explored the feasibility to obtain visible, infrared, hyperspectral and thermal 3D registrations of simulated crime scenes using photogrammetry for use in forensic practice. Raeva et al. (2019) carried out unmanned flights with a fixed-wing platform with two different sensors – multispectral and thermal in order to examine two main crops cultivated area. Turner et al. (2020) investigated geological discontinuities in hard rock masses using UAV-mounted thermal and multispectral cameras. Matese and Di Gennaro (2018) described the implementation of a multisensor UAV system capable of flying with three sensors simultaneously to present performances in the characterization of spatial variability in terms of vegetative vigor, water stress and missing plant detection.

When the studies in the literature are examined, it is seen that the geometric accuracy analysis of the photogrammetric models of different sensor images has not been considered concurrently. The scope of this study is to compare the photogrammetric three-dimensional point accuracies, point clouds and polygons produced using test area images of sensors having different spectral ranges and geometric resolutions. In this study, the three-dimensional test field images obtained with RGB, multispectral and thermal sensors were oriented photogrammetrically and the accuracies of the control points on the obtained models were compared. In particular, the effects of sensors on photogrammetry as a result of modeling with multispectral and thermal images were discussed.

2. METHODOLOGY

All photogrammetric experiments were carried out on the three-dimensional test field as shown in Fig. 1. The predefined coded targets of Photomodeler and Agisoft Metashape software have been fixed on the test area in dimensions of 85 cm x 85 cm x 20 cm. Providing depth variations in control points produces more reliable results during interior and exterior camera orientations (Fraser, 2013). In order to have higher accuracy, the ratio of test field depth to image shooting distance was determined as 0.25, while a nadir viewing angle was preferred.

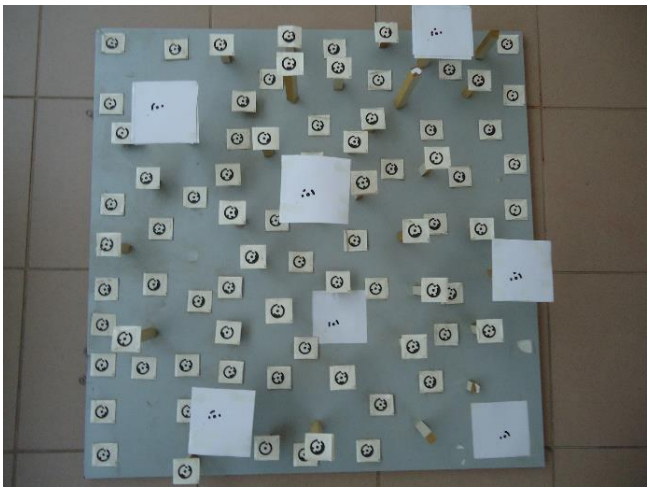

Figure 1. Three dimensional test field

As indicated in the workflow in Fig. 2, firstly, the coordinates of the control points were calculated on the test field using Sony RGB photogrammetric model. Then, photogrammetric models were created by taking test field images with Mapir Survey3 OCN multispectral and Optris PI 450 thermal cameras.

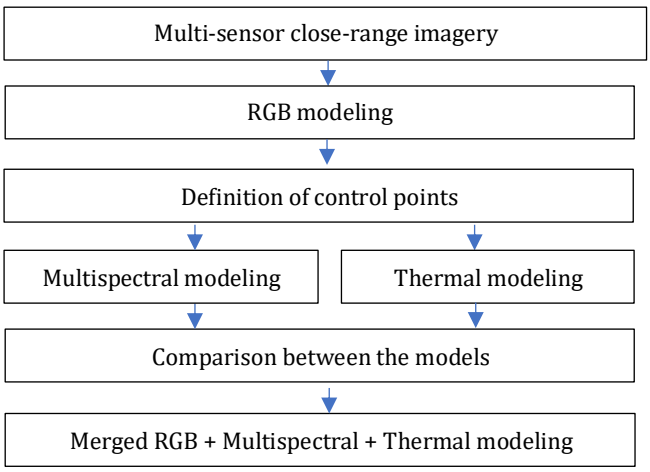

Figure 2. Workflow for photogrammetric analysis

The features of the cameras used in the study are shown in Table 1. Although the geometric resolutions of RGB cameras and multispectral cameras are close to each other, it is seen that the resolution of the thermal camera is quite low compared to the others. In the results section, the accuracies produced from photogrammetric models are presented. Finally, three photogrammetric models obtained using different sensor have been optimized and merged.

Table 1. Sensor specifications

Name	Bands	Resolution (pixel)	Spectral wavelength range (nm)
Sony	Red Green Blue	4320 x 3240	400 - 700
Mapir	Orange Cyan NIR	4000x3000	450 - 900
Optris	Thermal	382 x 288	(8 – 14) x10^3

2.1. Photogrammetric Control Points

The coordinates of the control points were also produced by the photogrammetric method. By using 10 images taken with the RGB camera, 75 coded targets were automatically measured with Photomodeler, then the orientation and bundle adjustment processes were completed. Modern bundle adjustment assessments and software solutions were discussed in Murtiyoso et al. (2018). Measurements of 7 coded targets (CP1, CP2, CP4, CP6, CP8, CP10 and CP12) belonging to Agisoft software were performed by manual photogrammetric method and model coordinates were generated. After the distance between the targets P1 and P8 was determined with a precision ruler, the model coordinate system was transformed into the local coordinate system defined in the metric system. In Agisoft software, 10 image orientations were re-processed with coded targets, and X, Y, Z coordinates of control points and their errors were defined as seen in Table 2. The table shows that the point location accuracies are between about 0.9 mm and 1.3 mm, while the elevation of the control points varies between 18.6 cm.

Table 2. Control points in the local coordinate system

No	X (m)	Y (m)	Z (m)	Error (m)
CP1	0.3750	-0.2895	-0.8057	0.0009
CP2	0.3557	0.0122	-0.6887	0.0013
CP4	0.0197	0.1448	-0.6212	0.0013
CP6	-0.1406	-0.2054	-0.6868	0.0011
CP8	0.0570	-0.0760	-0.8068	0.0012
CP10	0.2448	0.4398	-0.7356	0.0012
CP12	-0.2293	0.3003	-0.6830	0.0013

2.2. Multispectral and Thermal Models

First, radiometric calibration of the multispectral camera images was performed in order to build quantitative spectral and spatial representations of the test field (Guo et al., 2019). Reflectance calibration target was used during radiometric correction of multispectral images. The pixel values of the captured target image are compared with the known reflectance values of the targets. Mapir calibration software then transform the pixel values and thus calibrate the test field images. The 12 images obtained as a result of the calibration were automatically oriented and optimized by the coded targets in Agisoft software. In addition, dense point clouds were produced (de Lima et al., 2021) using oriented multispectral images as depicted in Fig. 3. It was observed that multispectral imagery enables orthophotos production as well as digital surface model.

Since 8 - 14 µm spectral range of thermal camera images is different than RGB and multispectral sensor images, it was not possible to automatically measure the coded targets in the Agisoft Metashape software. Due to noise and radiometric distortions on the thermal images, automatic feature detection and matching was not sufficient for orientation.

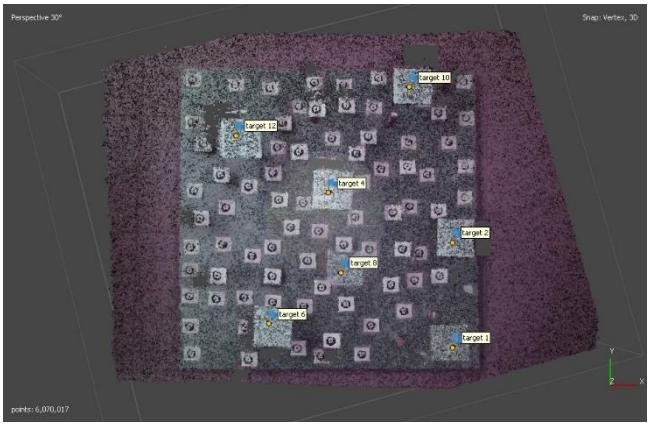

Figure 3. Multispectral dense cloud

Thermal image contents are also affected by different view angles of the camera and each object emits thermal radiation in a certain manner, as it changes its geometry (Athanasopoulos & Siakavellas. 2017). Fig. 4 shows the views of the same features in different orientated thermal images. 7 coded targets and 11 other targets were manually measured on 13 thermal images. Correct emissivity values could provide valuable information concerning the interpretation of thermal images obtained from thermographic surveys (Avdelidis & Moropoulou, 2003). The selectivity of some targets for manual measurements has been increased by metal coins. As the metal materials, have lower emissivity values, targets become more determined for image measurements in the thermal images.

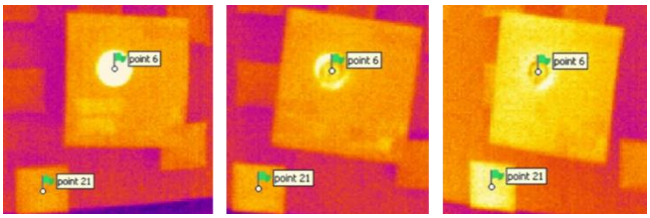

Figure 4. Same features on different thermal images

Beside the disadvantage of low geometric resolution, Fig. 5 explicitly depicts high distortion, low contrast and blur effect that reduce image quality dramatically (Mello Román et al., 2019). Therefore, the loss of details, which is an unavoidable result for thermal imagery, causes obstacles during three-

dimensional photogrammetric modeling process. Photogrammetric measurement points can also be seen in a thermal image in Fig. 5.

Another obstacle in thermal photogrammetry is outer heat sources occurred in scene during image taking. This situation leads to global noise effects in image frame. As seen in Fig. 5, at the right side of the image, purple, which represents lower emissivity whereas the top left corner brighter pixels, which represents higher emissivity due to external heat source.

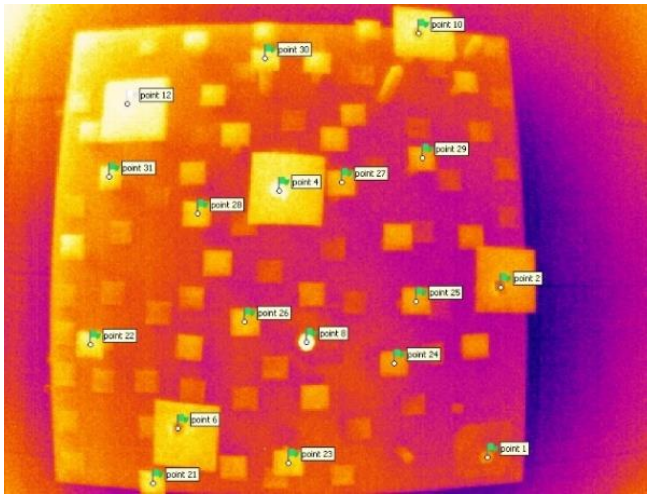

Figure 5. A thermal image and measurement points

By measuring manually a total of 18 common points on the images, orientation and optimization were implemented successfully (Fig. 5). Dense point clouds could not be produced due to insufficient automatic matching based on the thermal image. A dense surface can only be created by an intensive manual measurement based on the oriented thermal model; as it is beyond the scope of this study, sparse thermal point cloud was used during point cloud comparisons.

2.3. Fused Photogrammetric Model

Three photogrammetric models using RGB, multispectral and thermal images were reconsidered for an unified orientation and bundle adjustment in order to produce a fusion model. The purpose of the fusion model is to optimize separate photogrammetric models all together. It enables compare different spectral values of any point or location. The fusion model consists of 10 RGB images, 12 multispectral images and 13 thermal images were carried out using 54 manual and coded marking points, and 10459 auto-match tie points. Successively, dense point cloud having 6179491 points was obtained as depicted in Fig. 6. Points of dense point cloud were colored using three different sensor images, although points were mostly colored with RGB and multispectral data.

On the other hand, the mosaic of orthophotos, which contains more thermal patches, was automatically produced as shown in Fig 7. The resolution of the orthomosaics was calculated as 0.312 mm/pix. Fused model imply that the thermal images might be utilized during orthophotos production, even if single thermal model is not able to accomplish photogrammetric products such as dense point cloud, surface model and orthophotos.

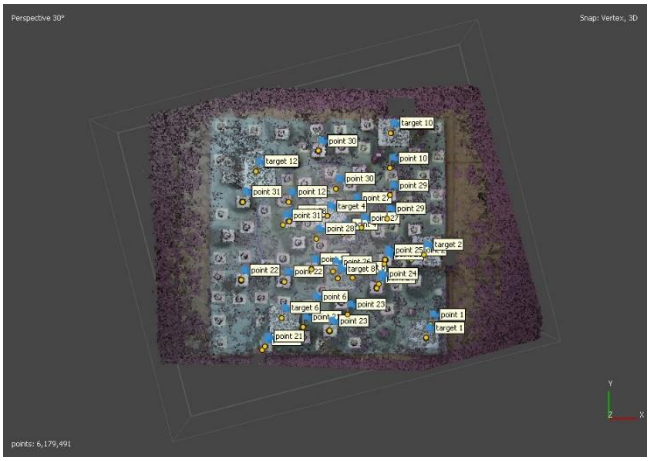

Figure 6. Dense cloud of fusion model

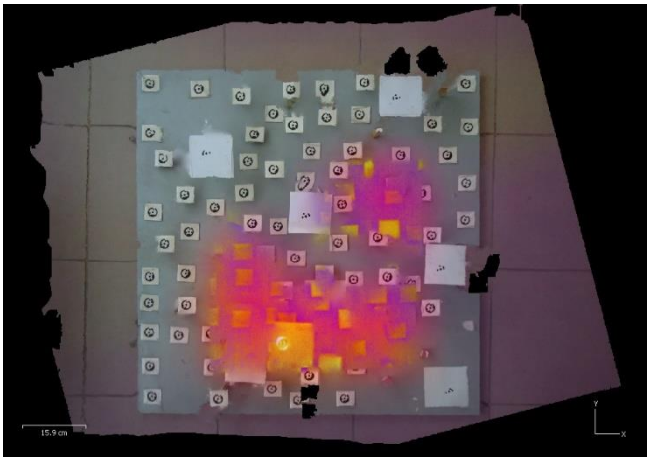

Figure 7. Orthomosaic of fusion model

3. RESULTS AND DISCUSSIONS

Photogrammetric models are evaluated in three subsections; first subsection regards control point measurement accuracies, second one is considered as evaluation of point cloud products whereas third one compares polygonal shapes.

3.1. Control Points Accuracies

When pixel errors were examined in Table 3 and Fig. 7, it is seen that photogrammetric measurement accuracies are similar in all image types. In other words, the accuracy of manual measurements made in thermal and automatic measurements in RGB and multispectral images produced similar results. In some control points, it is also observed that manual thermal measurements are better than automatic multispectral measurements. As a result, the lowest projection errors accomplished with RGB photogrammetric model.

However, when metric accuracies are analyzed in Table 4 and Fig. 8, it is seen that RGB and multispectral results differ significantly from thermal results. Although RGB stands out in terms of accuracy, the results obtained from multispectral images are also very consistent. This is due to the fact that one pixel size of

the thermal camera sensor is larger than other sensors. Table 5 describes differences of common control points between RGB model and multispectral models, while Table 6 explains differences between RGB and Thermal models. Results of coordinate differences prove that RGB and multispectral models are quite coherent. On the other hand, CP2, CP4 and CP12 are observed as the most biased points between the discussed models. The comparison of RGB and Thermal model indicate that CP2 and CP6 have more variance than other control points.

Table 3. Errors of control points obtained from different imagery models in pixel unit

No	RGB	Multispectral	Thermal
CP1	0.231	0.343	0.523
CP2	0.276	0.476	0.290
CP4	0.215	0.293	0.278
CP6	0.252	0.558	0.290
CP8	0.192	0.144	0.334
CP10	0.174	0.299	0.337
CP12	0.289	0.598	0.386

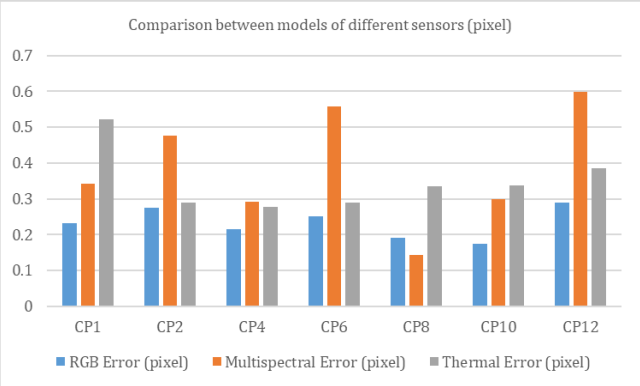

Figure 7. Comparison between in pixel unit

Table 4. Errors of control points in millimeter unit

No	RGB	Multispectral	Thermal
CP1	0.9	1.7	2.9
CP2	1.3	1.6	3.5
CP4	1.3	1.1	3.1
CP6	1.1	0.7	4.8
CP8	1.2	1.2	1.5
CP10	1.2	1.3	1.8
CP12	1.3	1.5	1.7

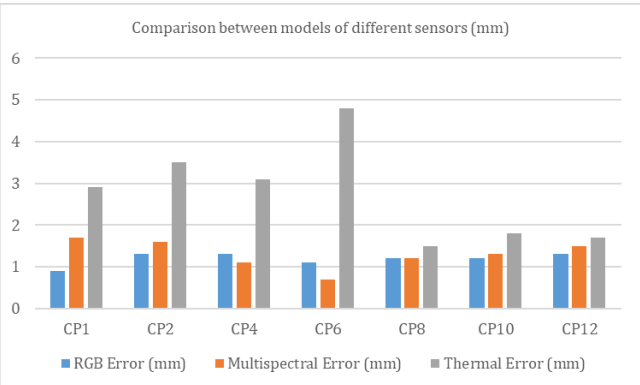

Figure 8. Comparison between errors in millimeter unit

Table 5. Differences of common control points between RGB model and multispectral models

No	ΔX (mm)	ΔY (mm)	ΔZ (mm)
CP1	+0.3	-0.7	-0.4
CP2	-0.9	+0.9	0.0
CP4	+0.6	+1.0	-0.6
CP6	+0.7	-0.8	+0.1
CP8	-0.6	-1.0	+0.1
CP10	-0.8	-0.5	+0.8
CP12	+0.7	+1.1	-0.2

In the study, as mentioned in methodology, the fusion model was also implemented considering RGB, multispectral and thermal images in one project. However, image measurements of control points in thermal image substantially diverge from other image measurements in the fusion model. Pixel errors in thermal images vary between 0.914 and 9.476 while errors in three-dimensional coordinate system differ between 11cm and 27 cm. The reason for the high deviations is that automatic coded target measurements cannot be performed in thermal images. Besides, tie points which detected using SIFT algorithm were also presented low matching accuracy among thermal images. Deviations of thermal image points from RGB image measurements can be observed in Fig. 9.

Table 6. Differences of common control points between RGB model and thermal models

No	ΔX (mm)	ΔY (mm)	ΔZ (mm)
CP1	+1.5	+0.6	+2.0
CP2	+1.4	+2.1	-2.2
CP4	+0.1	-0.3	+2.2
CP6	-2.6	+0.9	-2.9
CP8	-1.1	-2.4	+0.6
CP10	-0.9	-1.2	-0.8
CP12	+1.6	+0.4	+1.1

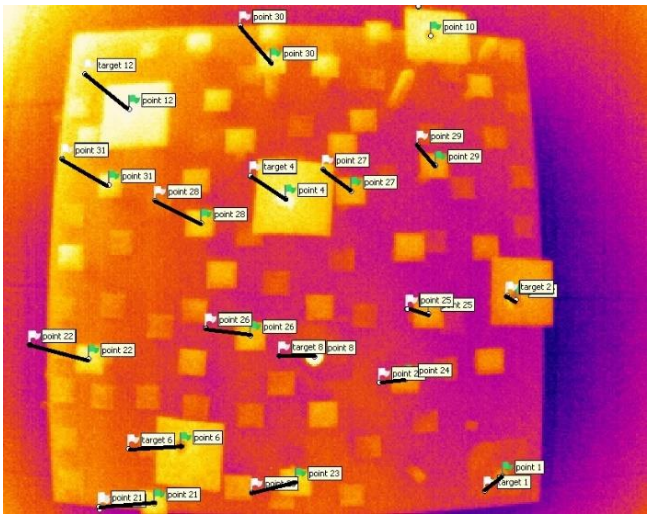

Figure 9. Deviations of thermal image points

3.2. Comparison of Point Clouds

Dense point clouds were produced from RGB and multispectral model as shown in Fig 10 and 11. However, thermal photogrammetric model was able to spare point cloud that represent test field (Fig. 12). The

dense point clouds were utilized for digital surface model production, which is essential for obtaining orthophotos. Thermal model was oriented and optimized, yet, digital surface model and orthophotos could not be accomplished from sparse point cloud. The only way getting thermal orthophotos is to use the fused model, however, it arises high measurement error issue for thermal images at that time. Another solution for thermal orthophotos production is increasing manual corresponding image point measurements, although it is a time consuming method in photogrammetry. Therefore sparse point cloud can be intensified so as to provide more discrete three-dimensional points for obtaining DSM models such as delaunay triangulation and inverse distance weighting (Wang et al., 2020).

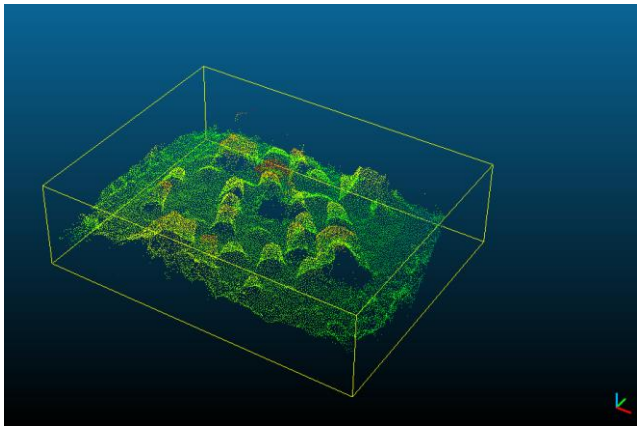

Figure 10. Dense point cloud of RGB model

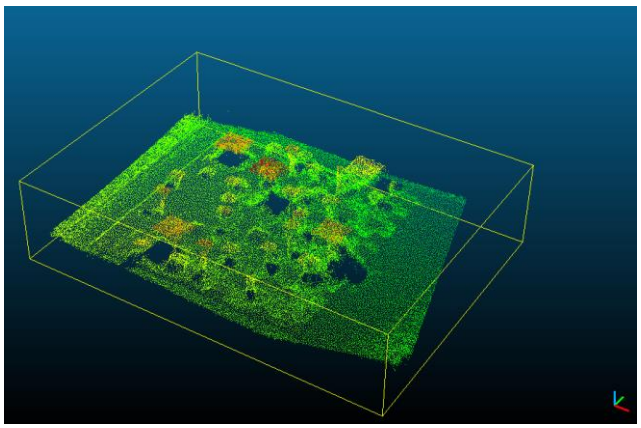

Figure 11. Dense point cloud of multispectral model

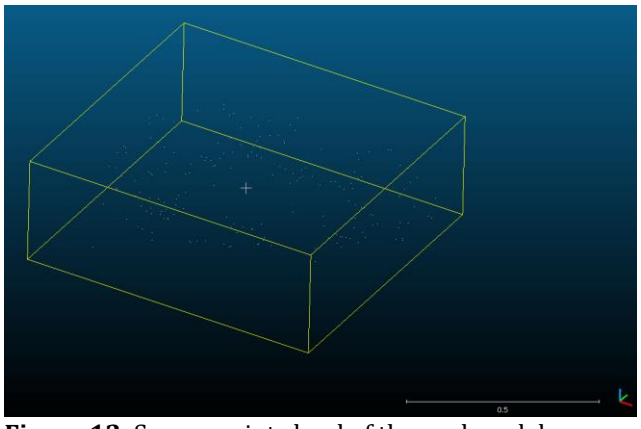

Figure 12. Sparse point cloud of thermal model

Number of point of RGB, multispectral and thermal clouds are 109489, 6069889 and 185, respectively. It is also seen that RGB and multispectral points' heights tend to similar distribution when their histogram analyzed (Fig. 13 and 14). In contrast to the dense point clouds, the distribution of the heights of sparse thermal points presents low sampling rates to represent the test field (Fig. 15). Consequently, thermal imagery using 382 x 288 resolution camera leads significant challenges as concerning multi sensor photogrammetric modelling.

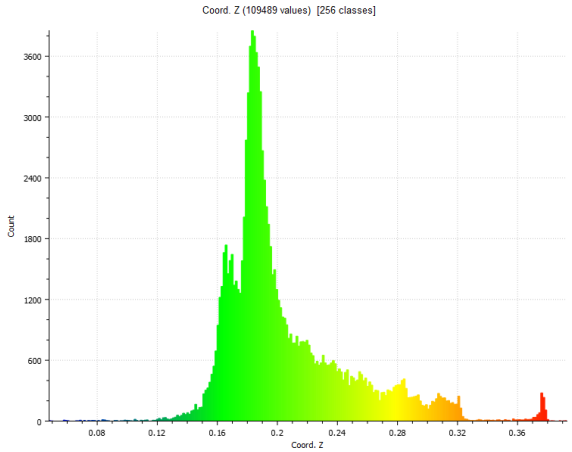

Figure 13. The distribution of Z coordinates of RGB dense point cloud

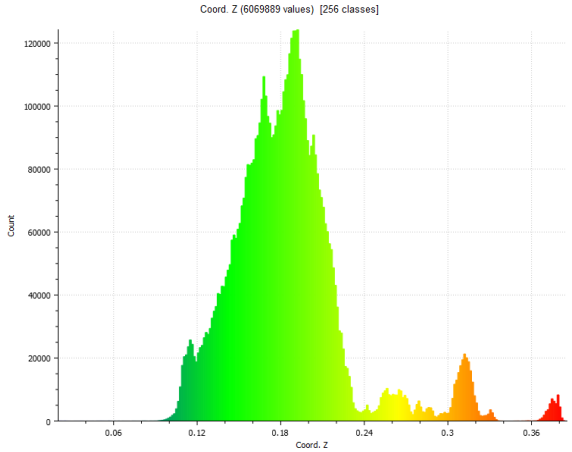

Figure 14. The distribution of coordinates Z of multispectral dense point cloud

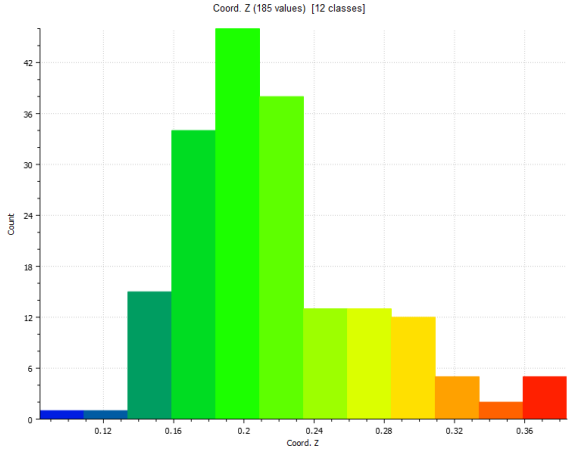

Figure 15. The distribution of coordinates Z of thermal sparse point cloud

The section (Section 1) and its four cross sections (CS1, CS2, CS3, and CS4) (Fig. 16) was determined on the test field and, then, Z values extracted from RGB and multispectral point clouds. In Fig. 17, Z coordinate values of RGB and multispectral points are represented as green and red lines, respectively.

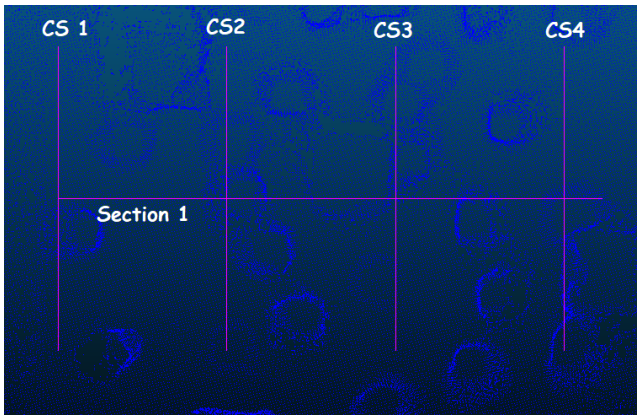

Figure 16. Section 1 and its four cross sections CS1, CS2, CS3 and CS4

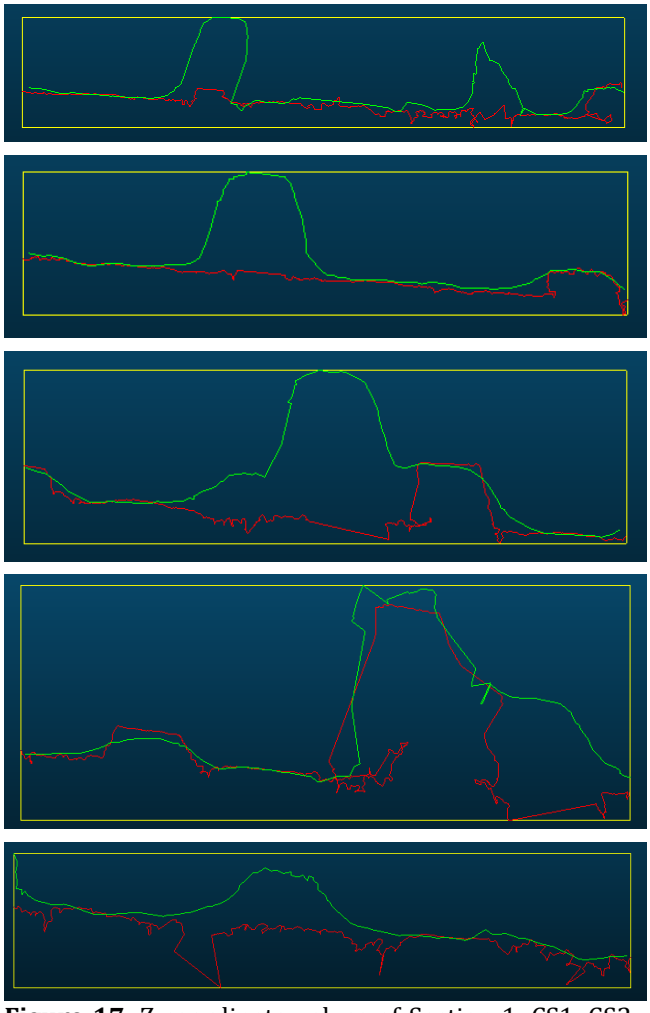

Figure 17. Z coordinate values of Section 1, CS1, CS2, CS3 and CS4 from RGB and multispectral point clouds are presented from top to down

3.3. Comparison of Extracted Polygons

Photogrammetry is also one of the important geometric data sources such as lines and polygons for geospatial applications. Therefore, in the scope of this study, polygons were created manually from photogrammetric models and their perimeters and areas were compared (Table 7). Polygons were obtained from 8 photogrammetric point vertices (CP1, CP2, CP10, CP12, CP21, CP22, CP30, CP31). Results show that all models presents significant metric accuracy as perimeter differences between polygons of RGB and the other models are 2 mm and 14 mm. Areas of polygons also validate coherence among multi-sensor models.

Table 7. Calculated measures of polygons

Model type	Perimeter (mm)	Area (cm²)
Polygon-RGB	2449	3997
Polygon-Multispectral	2451	3995
Polygon-Thermal	2463	4072

4. CONCLUSIONS

In photogrammetry, besides three-dimensional RGB models, multispectral and thermal models were successfully produced. In particular, radiometric corrections on multispectral and thermal images are important in terms of geometric positioning accuracy. Due to the difficulties in automatic processing of thermal images, mandatory manual point measurement causes a time-consuming model production and accuracy losses. The low resolution of thermal images makes it difficult to combine and analyze them with RGB and multispectral models. In the future, new thermal photogrammetric studies which deal data fusion with RGB and multispectral camera images should be carried out to increase the resolution of thermal models. The fused photogrammetric model was produced successfully, however specific approaches need to be developed in order to increase model performance and product quality.

Conflicts of interest:

The authors declare no conflicts of interest.

REFERENCES

Athanasopoulos N & Siakavellas N J (2017). Smart patterned surfaces with programmable thermal emissivity and their design through combinatorial strategies. Scientific reports, 7(1), 1-16.

Avdelidis N P & Moropoulou A (2003). Emissivity considerations in building thermography. Energy and Buildings, 35(7), 663-667.

Biass S Orr T R, Houghton B F, Patrick M R, James M R & Turner N (2019). Insights into pāhoehoe lava emplacement using visible and thermal structure-from-motion photogrammetry. Journal of Geophysical Research: Solid Earth, 124(6), 5678-5695.

Candiago S, Remondino F, De Giglio M, Dubbini M & Gattelli M (2015). Evaluating multispectral images and vegetation indices for precision farming applications from UAV images. Remote sensing, 7(4), 4026-4047.

de Lima R S, Lang M, Burnside N G, Peciña M V, Arumäe T, Laarmann D, ... & Sepp K (2021). An Evaluation of the Effects of UAS Flight Parameters on Digital Aerial Photogrammetry Processing and Dense-Cloud Production Quality in a Scots Pine Forest. Remote Sensing, 13(6), 1121.

Edelman G J & Aalders M C (2018). Photogrammetry using visible, infrared, hyperspectral and thermal imaging of crime scenes. Forensic science international, 292, 181-189.

Erenoglu R C, Akcay O & Erenoglu O (2017). An UAS-assisted multi-sensor approach for 3D modeling and reconstruction of cultural heritage site. Journal of cultural heritage, 26, 79-90.

Fraser C S (2013). Automatic camera calibration in close range photogrammetry. Photogrammetric Engineering & Remote Sensing, 79(4), 381-388.

Guo Y, Senthilnath J, Wu W, Zhang X, Zeng Z & Huang H (2019). Radiometric calibration for multispectral camera of different imaging conditions mounted on a UAV platform. Sustainability, 11(4), 978.

Matese A & Di Gennaro S F (2018). Practical applications of a multisensor UAV platform based on multispectral, thermal and RGB high resolution images in precision viticulture. Agriculture, 8(7), 116.

Mello Román J C, Vázquez Noguera J L, Legal-Ayala H, Pinto-Roa D P, Gomez-Guerrero S & García Torres M (2019). Entropy and contrast enhancement of infrared thermal images using the multiscale top-hat transform. Entropy, 21(3), 244.

Minařík R & Langhammer J (2016). Use of a multıspectral uav photogrammetry for detectıon and trackıng of forest dısturbance dynamıcs. International Archives of the Photogrammetry, Remote Sensing & Spatial Information Sciences, 41.

Murtiyoso A, Grussenmeyer P, Börlin N, Vandermeerschen J & Freville T (2018). Open source and independent methods for bundle adjustment assessment in close-range UAV photogrammetry. Drones, 2(1), 3.

Nebiker S, Annen A, Scherrer M & Oesch D (2008). A light-weight multispectral sensor for micro UAV—Opportunities for very high resolution airborne remote sensing. Int. Arch. Photogramm. Remote Sens. Spat. Inf. Sci, 37(B1), 1193-1200.

Raeva P L, Šedina J & Dlesk A (2019). Monitoring of crop fields using multispectral and thermal imagery from UAV. European Journal of Remote Sensing, 52(sup1), 192-201.

Ribeiro-Gomes K, Hernández-López D, Ortega J F, Ballesteros R, Poblete T & Moreno M A (2017). Uncooled thermal camera calibration and optimization of the photogrammetry process for UAV applications in agriculture. Sensors, 17(10), 2173.

Sankey J B, Sankey T T, Li J, Ravi S, Wang G, Caster J & Kasprak A (2021). Quantifying plant-soil-nutrient dynamics in rangelands: Fusion of UAV hyperspectral-LiDAR, UAV multispectral-photogrammetry, and ground-based LiDAR-digital photography in a shrub-encroached desert grassland. Remote Sensing of Environment, 253, 112223.

Saura J R, Reyes-Menendez A & Palos-Sanchez P (2019). Mapping multispectral Digital Images using a Cloud Computing software: applications from UAV images. Heliyon, 5(2), e01277.

Turner R M, MacLaughlin M M & Iverson S R (2020). Identifying and mapping potentially adverse discontinuities in underground excavations using thermal and multispectral UAV imagery. Engineering Geology, 266, 105470.

Van der Sluijs J, Kokelj S V, Fraser R H, Tunnicliffe J & Lacelle D (2018). Permafrost terrain dynamics and infrastructure impacts revealed by UAV photogrammetry and thermal imaging. Remote Sensing, 10(11), 1734.

Wakeford Z E, Chmielewska M, Hole M J, Howell J A & Jerram D A (2019). Combining thermal imaging with photogrammetry of an active volcano using UAV: an example from Stromboli, Italy. The Photogrammetric Record, 34(168), 445-466.

Wang J, Wang L, Jia M, He Z & Bi L (2020). Construction and optimization method of the open-pit mine DEM based on the oblique photogrammetry generated DSM. Measurement, 152, 107322.

Webster C, Westoby M, Rutter N & Jonas T (2018). Three-dimensional thermal characterization of forest canopies using UAV photogrammetry. Remote Sensing of Environment, 209, 835-847.

Wewel F, Scholten F & Gwinner K (2000). High resolution stereo camera (HRSC)-multispectral 3D-data acquisition and photogrammetric data processing. Canadian Journal of Remote Sensing, 26(5), 466-474.

Xu Z, Shen X, Cao L, Coops N C, Goodbody T R, Zhong T, ... & Wu X (2020). Tree species classification using UAS-based digital aerial photogrammetry point clouds and multispectral imageries in subtropical natural forests. International Journal of Applied Earth Observation and Geoinformation, 92, 102173.

Zefri Y, ElKettani A, Sebari I & Ait Lamallam S (2018). Thermal infrared and visual inspection of photovoltaic installations by UAV photogrammetry—application case: morocco. Drones, 2(4), 41.

Zumr D, David V, Jeřábek J, Noreika N & Krása J (2020). Monitoring of the soil moisture regime of an earth-filled dam by means of electrical resistance tomography, close range photogrammetry, and thermal imaging. Environmental Earth Sciences, 79(12), 1-11.